2020

Analysis of Iron Sources in Antarctic Continental Shelf Waters

Michael S. Dinniman
Old Dominion University, msd@ccpo.odu.edu

Pierre St-Laurent
Old Dominion University, pstlaure@odu.edu

Kevin R. Arrigo

Eileen E. Hofmann
Old Dominion University, ehofmann@odu.edu

Gert L. van Dijken

Original Publication Citation

Dinniman, M. S., St-Laurent, P., Arrigo, K. R., Hofmann, E. E., & van Dijken, G. L. (2020). Analysis of iron sources in antarctic continental shelf waters. *Journal of Geophysical Research: Oceans, 125*(5), 19 pp., Article e2019JC015736. https://doi.org/10.1029/2019JC015736

JGR Oceans

RESEARCH ARTICLE
10.1029/2019JC015736

Analysis of Iron Sources in Antarctic Continental Shelf Waters

Michael S. Dinniman[1], Pierre St-Laurent[1], Kevin R. Arrigo[2], Eileen E. Hofmann[1], and Gert L. van Dijken[2]

[1]Center for Coastal Physical Oceanography, Old Dominion University, Norfolk, VA, USA, [2]Department of Earth System Science, Stanford University, Stanford, CA, USA

Key Points:
- Transport of four sources of dissolved iron is simulated with a circum-Antarctic ocean/sea ice/ice shelf circulation model
- Correlations between satellite-derived chlorophyll and simulated dissolved iron confirm that productivity is linked to ice shelf basal melt
- Shelf circulation changes driven by ice shelf basal melt are more important for dissolved iron supply than direct supply by meltwater

Supporting Information:
- Supporting Information S1

Correspondence to:
M. S. Dinniman,
msd@ccpo.odu.edu

Citation:
Dinniman, M. S., St-Laurent, P., Arrigo, K. R., Hofmann, E. E., & van Dijken, G. L. (2020). Analysis of iron sources in Antarctic continental shelf waters. *Journal of Geophysical Research: Oceans*, *125*, e2019JC015736. https://doi.org/10.1029/2019JC015736

Received 3 OCT 2019
Accepted 20 APR 2020
Accepted article online 23 APR 2020

Abstract Previous studies showed that satellite-derived estimates of chlorophyll *a* in coastal polynyas over the Antarctic continental shelf are correlated with the basal melt rate of adjacent ice shelves. A 5-km resolution ocean/sea ice/ice shelf model of the Southern Ocean is used to examine mechanisms that supply the limiting micronutrient iron to Antarctic continental shelf surface waters. Four sources of dissolved iron are simulated with independent tracers, assumptions about the source iron concentration for each tracer, and an idealized summer biological uptake. Iron from ice shelf melt provides about 6% of the total dissolved iron in surface waters. The contribution from deep sources of iron on the shelf (sediments and Circumpolar Deep Water) is much larger at 71%. The relative contribution of dissolved iron supply from basal melt driven overturning circulation within ice shelf cavities is heterogeneous around Antarctica, but at some locations, such as the Amundsen Sea, it is the primary mechanism for transporting deep dissolved iron to the surface. Correlations between satellite chlorophyll *a* in coastal polynyas around Antarctica and simulated dissolved iron confirm the previous suggestion that productivity of the polynyas is linked to the basal melt of adjacent ice shelves. This correlation is the result of upward advection or mixing of iron-rich deep waters due to circulation changes driven by ice shelf melt, rather than a direct influence of iron released from melting ice shelves. This dependence highlights the potential vulnerability of coastal Antarctic ecosystems to changes in ice shelf basal melt rates.

Plain Language Summary Phytoplankton in Antarctic coastal waters grow more rapidly relative to waters farther offshore. This growth is limited by the availability of light for photosynthesis and the supply of the micronutrient dissolved iron. Earlier studies suggest that satellite-based estimates of phytoplankton growth are related to the melting of nearby floating portions (called ice shelves) of the Antarctic ice sheet. In this study, a computer model, which includes melting of ice shelves, is used to examine the different sources of dissolved iron that supply the well-lit summer surface waters around Antarctica. Dissolved iron is available in the floating ice shelves, and the direct supply of this iron to coastal waters by melting of the bottom of the ice shelf is important for enhancing biological production. However, melting creates less dense water at the ice shelf base that rises and brings deep waters that contain dissolved iron towards the surface in front of the ice shelf. The model shows that this input provides a larger source of dissolved iron to the open surface waters in many coastal regions than does direct supply from the ice shelf meltwater. This implies that phytoplankton growth may be vulnerable to changes in ice shelf basal melt.

1. Introduction

The high productivity of Antarctic continental shelf waters (Arrigo et al., 1998; Arrigo et al., 2008) is in large part due to the many coastal polynyas that form on the shelf. Coastal polynyas are areas along the shoreline of open water surrounded by sea ice. These polynyas are maintained throughout much of the year either by upwelling of warm water or sea ice removal by offshore-directed continental winds (Morales Maqueda et al., 2004). Polynyas provide an ice-free environment in early spring when solar radiation is increasing, which supports phytoplankton concentrations that are considerably higher than the surrounding ice-covered waters (Arrigo & van Dijken, 2003). Summer sea ice melt provides vertical stratification that retains the primary producers in the relatively well-lit surface waters. The resultant phytoplankton blooms persist even after sea ice has disappeared in summer (Arrigo & van Dijken, 2003). The enhanced biological productivity of coastal polynyas supports rich ecosystems and the highest densities of upper trophic level

organisms in the Southern Ocean (Karnovsky et al., 2007; Smetacek & Nichol, 2005; Stirling, 1997). This productivity also increases the efficiency of the local biological pump, making areas like the Ross Sea polynya large sinks of anthropogenic carbon dioxide (Arrigo et al., 2008).

Phytoplankton growth and abundance in Antarctic coastal waters are limited by the availability of light and trace metals, primarily dissolved iron (dFe) (Boyd, 2002; Boyd et al., 2012; De Baar et al., 1990; Martin et al., 1990). The input of dFe by atmospheric deposition of terrestrially derived iron-rich dust (Mahowald et al., 2009) to Antarctic coastal regions is generally minimal because of the isolation from terrestrial sources (Boyd et al., 2012), although there are locations where this input is significant and may become more important in the future (Duprat et al., 2019). Dissolved Fe concentrations increase with proximity to the Antarctic coast (Sedwick et al., 2008) and continental shelf waters are especially enriched by input from Fe-rich sediments (Fitzwater et al., 2000; Gerringa et al., 2012). However, dFe concentrations in Antarctic shelf waters are insufficient to promote complete utilization of macronutrients by phytoplankton (Arrigo et al., 2000; Mills et al., 2012; Smith & Gordon, 1997). As a result, processes that enhance dFe inputs to Antarctic coastal waters generally increase phytoplankton production and abundance (De Baar et al., 1990; Fitzwater et al., 2000; Martin et al., 1990).

Arrigo et al. (2015) examined the relative importance of a number of environmental variables on satellite-derived estimates of chlorophyll *a* (Chl *a*) concentration and rates of net primary production (NPP) in 46 coastal polynyas around Antarctica. The variables examined include mean daily photosynthetically usable radiation, number of open water days, open water area, sea surface temperature, continental shelf width, and basal melt rate of adjacent ice shelves. The 46 polynyas cover most of the area of the Antarctic continental shelf that is significantly ice free during the summer where light penetrates the surface ocean. Arrigo et al. (2015) found that ice shelf basal melt rates explained 59% of the between-polynya variance in mean Chl *a* concentration and explained twice as much of the variance as the next most important variable, thus suggesting that the productivity of coastal polynyas is sensitive to the release of dFe from melting ice shelves. However, the detail of how ice shelf meltwater directly or indirectly supplies dFe to the polynyas is still an open question.

The cryosphere is a potentially important source of dFe to Antarctic surface waters through melting of sea ice or floating (ice shelves and icebergs) glacial ice. The cryosphere also indirectly supplies iron by affecting coastal circulation. The formation of sea ice in coastal polynyas leads to deep vertical mixing over the continental shelf. This mixing allows sediment-derived iron or iron-rich Circumpolar Deep Water (CDW), which intrudes onto the Antarctic continental shelf below the pycnocline, to be mixed into surface waters prior to the growing season (Mack et al., 2017; McGillicuddy et al., 2015). Basal melting of ice shelves can drive a buoyancy-forced overturning circulation within ice shelf cavities (Greisman, 1979). This "meltwater pump" can significantly modify the circulation outside the ice shelf cavity (Jourdain et al., 2017) and can also transport iron-rich deep water to the surface through a three-dimensional pathway rather than purely one-dimensional vertical mixing (St-Laurent et al., 2017).

This study assesses the relative importance of four dFe sources (ice shelf melt, sediments, CDW, and sea ice melt) to Antarctic continental shelf surface waters, including the direct and indirect contributions from the cryosphere. This assessment is based on simulations from a primitive equation ocean/sea ice/ice shelf circulation model of the Southern Ocean and includes examination of sensitivity to the wide range of reported iron concentrations in glacial sources. Satellite-derived estimates of Chl *a* and NPP provide verification of the simulated patterns of dFe supply.

2. Circulation Model and Tracer Simulations

2.1. Circum-Antarctic Model Structure and Implementation

The circum-Antarctic circulation model used in this study (Dinniman et al., 2015; Dinniman et al., 2016) is an implementation of the Regional Ocean Modeling System, which is a primitive equation finite volume model with a terrain following vertical coordinate system (Haidvogel et al., 2008; Shchepetkin & McWilliams, 2009). The model includes a dynamic sea-ice model (Budgell, 2005), and the mechanical and thermodynamic interactions between floating ice shelves and the water underneath (Dinniman et al., 2011; Holland & Jenkins, 1999) are simulated as described in Dinniman et al. (2015).

The circum-Antarctic model domain (Figure 1) encompasses the entire Antarctic continental shelf including the portion (~35%) underneath the floating ice shelves. The domain extends northward from the continent across Drake Passage to South America and is north of the maximum winter sea ice extent. The model grid uses a polar stereographic projection. The model has 32 vertical levels with smaller spacing near the surface and bottom and a mean thickness of 1.65 m for the surface level over the open Antarctic continental shelf (not underneath an ice shelf). The model topography (ocean bathymetry and ice shelf cavities) for the 5-km horizontal resolution domain used here is from the RTopo-2 dataset (Schaffer et al., 2016), with additional updates in the Amundsen Sea Embayment (Millan et al., 2017).

The initial implementation of the circum-Antarctic model, which used a 10-km horizontal resolution grid and ERA-Interim reanalysis atmospheric forcing (Dee et al., 2011), accurately simulated sea ice concentrations, eddy kinetic energy in the Antarctic Circumpolar Current, and the basal melt of the larger cold water ice shelves around Antarctica (Dinniman et al., 2015). Increasing the horizontal resolution to 5 km improved the temperature simulation for the Amundsen/Bellingshausen continental shelf (Dinniman et al., 2016) and enhanced ice shelf basal melt rates in the area, consistent with other modeling studies that showed improvements in the Amundsen deep shelf temperatures with similar resolution changes (Nakayama et al., 2014). The current 5-km model with the upgraded bathymetry more accurately simulates the transport of warm CDW onto the continental shelf in some areas of West Antarctica (Dinniman et al., 2016), which increases the basal melt rate for several warm water ice shelves in the Amundsen and Bellingshausen Seas (Table 1). Increasing the horizontal resolution to a 1-km scale would likely further increase the basal melt rate for the warm water shelves (i.e., Graham et al., 2016). The basal melt rates of the larger cold water ice shelves remain similar.

The dynamic sea ice model (Budgell, 2005) is based on two-layer ice thermodynamics (and a molecular sublayer beneath the sea ice) described by Mellor and Kantha (1989) and Häkkinen and Mellor (1992). A snow layer is included, as well as a conversion of snow to ice when the snow-ice interface is below sea level, along with a simple estimate of frazil ice production (Steele et al., 1989). Ice dynamics are based on an elastic-viscous-plastic rheology (Hunke, 2001; Hunke & Dukowicz, 1997). The ice model has one thickness category, which is adequate because of the limited extent of multiyear ice in the Antarctic (Comiso, 2010). This sea ice model has been shown to accurately simulate sea ice concentrations, including coastal polynyas, in many regional implementations around Antarctica (Dinniman et al., 2015, 2018; Stern et al., 2013; St-Laurent et al., 2017).

For the time span of the simulations used in this study (less than a decade), the modeled ice shelves are assumed to be static; thinning (or thickening) of the ice shelf and iceberg calving are not included. The model simulates mechanical (surface drag and depressed ocean free surface) and thermodynamic (heat and salt fluxes due to ice melting and freezing) interactions between the floating ice shelves and the water underneath (Dinniman et al., 2011; Holland & Jenkins, 1999). Open ocean momentum, heat, and fresh water (imposed as a salt flux) fluxes are calculated from the COARE 3.0 bulk flux algorithm (Fairall et al., 2003) with no relaxation of surface temperature or salinity to a specified field. Vertical momentum and tracer mixing are computed using the K-profile parameterization (Large et al., 1994) but modified such that the surface boundary layer depth under stabilizing conditions with nonzero surface shortwave flux is set to a minimum depth, equal to the directly wind-forced minimum depth under stable conditions in a Kraus–Turner bulk mixed-layer model (Dinniman et al., 2012; Niiler & Kraus, 1977). Ocean tides are not included. Additional details of the circum-Antarctic model are given in Dinniman et al. (2015).

The circum-Antarctic simulation used in this study starts after a six-year model initialization/spin-up, similar to the approach used for the 10-km model (Dinniman et al., 2015). Lateral boundary conditions for temperature, salinity, velocities, and sea surface height are the same as in Dinniman et al. (2015). The model open boundaries extend northward of the sea ice extent observed during the satellite era (1979 to present), thereby removing the need to specify sea ice boundary information. The model is run for 7 years using the same base case atmospheric forcing (ERA-Interim reanalysis [Dee et al., 2011] winds, 2-m air temperatures, sea level pressure, and relative humidity; Global Precipitation Climatology Project [Adler et al., 2003] precipitation; and International Satellite Cloud Climatology Project [Rossow et al., 1996] cloud fraction) as in Dinniman et al. (2015). Atmospheric data are from 2010, and the simulation is forced by continuously repeating 2010 conditions to asses model drift and externally forced variability in producing interannual

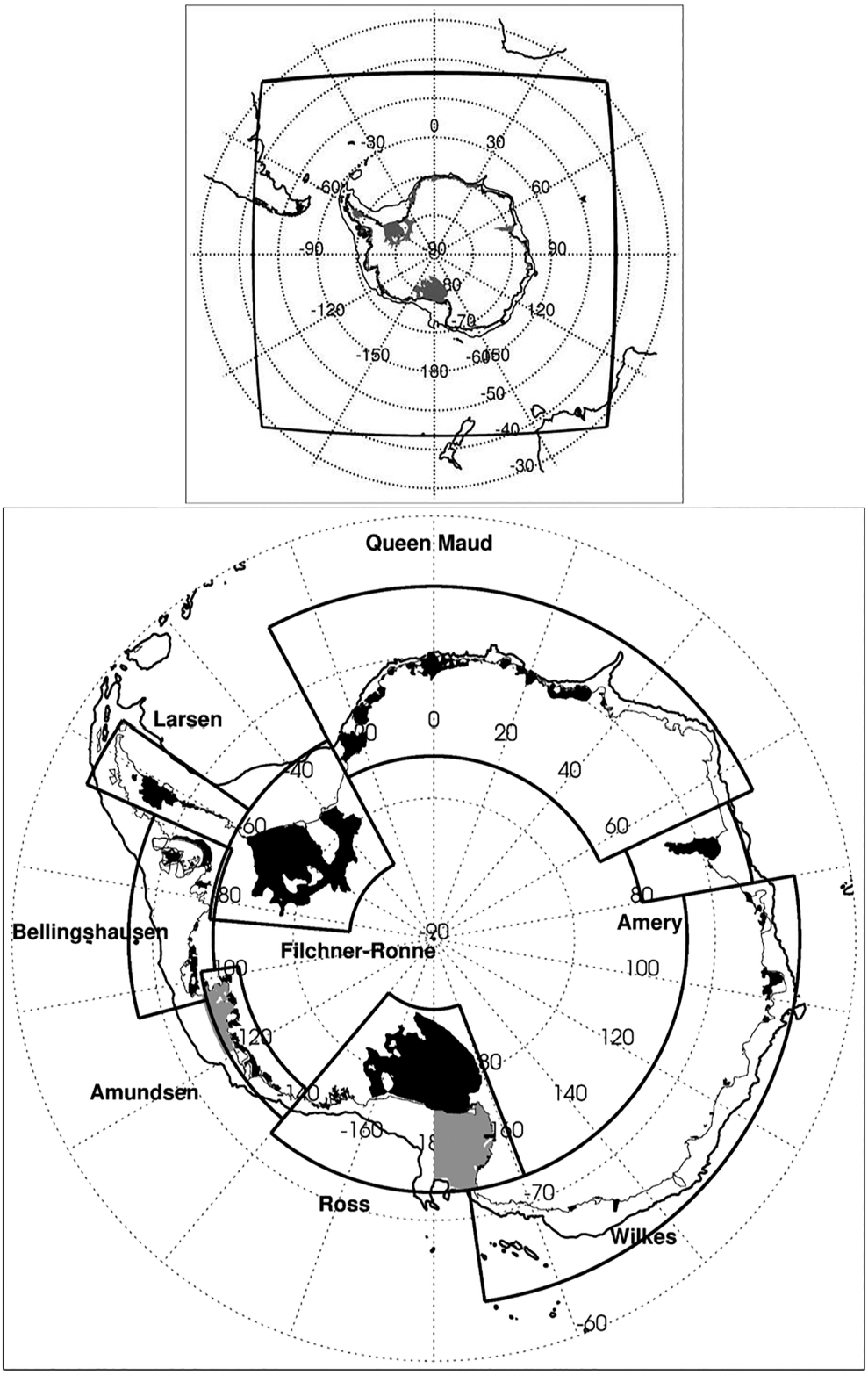

Figure 1. Top panel: Map showing the extent of the circum-Antarctic model domain (outer solid line). Gray shaded areas are the model floating ice shelves. Bottom panel: Expanded view of the model domain over the Antarctic continental shelf showing the eight sectors used for the ice shelf melt water tracers (black solid lines). The ice shelves included in the model (black shaded areas) and the western Ross Sea and eastern Amundsen Sea continental shelf areas used for simulation analysis (gray shaded areas) are shown. The 1,500-isobath is also shown (thin black line).

Table 1
Comparison of Simulated Basal Melt Obtained With Implementations of the Circum-Antarctic Model Using 10-km (Dinniman et al., 2015) and 5-km (this study) resolution to observational-based estimates for the entire continent (total: Gt year^{-1}) and the larger Antarctic ice shelves (m yr^{-1})

Ice shelf	Basal melt (10-km) Gt year^{-1}; m yr^{-1}	Basal melt (5-km) Gt year^{-1}; m yr^{-1}	Observation-based estimate Gt year^{-1}; m yr^{-1}	Reference
Total	664	826	756	Jacobs et al., 1996
			1,027	Rignot & Jacobs, 2008
			1,280–1,628	Depoorter et al., 2013
			1,090–1,560	Rignot et al., 2013
			1,410–1,622	Liu et al., 2015
Amery	1.10 ± 0.54	0.61 ± 0.25	0.71–0.97	Wen et al., 2010
			0.36–0.62	Yu et al., 2010
			0.30–1.00	Depoorter et al., 2013
			0.2–1.0	Rignot et al., 2013
			1.66	Liu et al., 2015
			0.6–1.4	Herraiz-Borreguero, Church, et al., 2016
Ross	0.14 ± 0.06	0.22 ± 0.08	0.18	Smethie & Jacobs, 2005
			0.07–0.11	Loose et al., 2009
			0.02–0.12	Depoorter et al., 2013
			0.0–0.2	Rignot et al., 2013
			0.06	Liu et al., 2015
Getz	0.66 ± 0.30	2.98 ± 1.02	1.1–4.6	Jacobs et al., 2013
			3.5–4.7	Depoorter et al., 2013
			3.9–4.7	Rignot et al., 2013
			4.82	Liu et al., 2015
Pine Island	1.62 ± 0.97	6.72 ± 1.11	20–28	Rignot, 1998
			22–33	Jacobs et al., 2011
			13.6–18.2	Depoorter et al., 2013
			15.2–17.2	Rignot et al., 2013
			14.00	Liu et al., 2015
Abbot	0.34 ± 0.18	0.90 ± 0.27	2.4–3.1	Depoorter et al., 2013
			1.1–2.3	Rignot et al., 2013
			1.17	Liu et al., 2015
George VI	1.19 ± 0.18	3.74 ± 0.53	2.1	Potter & Paren, 1985
			2.8	Corr et al., 2002
			3.1–4.8	Jenkins & Jacobs, 2008
			2.6–3.2	Depoorter et al., 2013
			3.1–4.5	Rignot et al., 2013
			4.02	Liu et al., 2015
			1.3–5.1	Adusumilli et al., 2018
Larsen C	0.35 ± 0.14	0.47 ± 0.14	0.16–0.44	Depoorter et al., 2013
			−0.6(mass gain)-1.4 (mass loss)	Rignot et al., 2013
				Liu et al., 2015
			1.04	Adusumilli et al., 2018
			−0.9(mass gain)-1.9 (mass loss)	
Filchner-Ronne	0.19 ± 0.02	0.24 ± 0.03	0.24–0.44	Nicholls et al., 2003
			0.20–0.34	Nicholls et al., 2009
			0.03–0.21	Depoorter et al., 2013
			0.2–0.4	Rignot et al., 2013
			0.02	Liu et al., 2015
Brunt + Riiser-Larsen	0.67 ± 0.43	0.50 ± 0.33	0.13–0.53	Depoorter et al., 2013
			−0.1(mass gain)-0.3 (mass loss)	Rignot et al., 2013
			0.27	Liu et al., 2015

Table 1
(continued)

Ice shelf	Basal melt (10-km) Gt year^{-1}; m yr^{-1}	Basal melt (5-km) Gt year^{-1}; m yr^{-1}	Observation-based estimate Gt year^{-1}; m yr^{-1}	Reference
Fimbul + Jelbart	1.51 ± 1.13	1.23 ± 0.75	0.25–0.79	Depoorter et al., 2013
			0.2–0.7	Rignot et al., 2013
			1	Langley et al., 2014
			0.77	Liu et al., 2015

Note. The range for the simulated estimates is the standard deviation of the 5-day averages that mostly reflects seasonal variability.

changes in the simulated circulation. The year 2010 is used because ice extent around the continent is typical, with all months between 92% and 108% of the climatological (1981–2010) ice extent of each month (Dinniman et al., 2015).

2.2. Tracer Implementation

Fourteen independent numerical tracers (Table 2) were used to simulate patterns of input of different dFe sources to Antarctic continental shelf waters (e.g., McGillicuddy et al., 2015). The tracers are assumed to be conservative, do not affect each other, and advect and diffuse similar to the active tracers (temperature and salinity) but without affecting the sea water density or circulation. Some of the tracers represent the same physical sources of dFe (e.g., dFe_{SED} and dFe_{SED_ZC}) but are used to test different hypotheses. Explicit biogeochemical transformation processes are not simulated, but simple parameterizations (detailed below) are used to estimate dFe removal. It is assumed that all dFe has been organically complexed to keep it in solution (e.g., Gledhill & Buck, 2012). Other than the sediment source (see below), the model tracks the tracer concentration. The conversion to a dFe concentration is done as postprocessing by attributing a temporally constant end member concentration (i.e., dFe value in the original unmodified source water) to each source, which allows for easily varying of some of the less well constrained end member values (see section 3.2). The tracer units are proportional to freshwater concentration for sea ice and ice shelf melt and are arbitrary for CDW (see below).

The inputs of dFe from glacial meltwater derived from floating ice shelves are simulated using tracers (Table 2) that are initialized in eight sectors (Figure 1; approximately the same sectors as in Paolo et al. (2015)) of the Antarctic ice sheet. The separate sectors allow estimation of local versus remote ice shelf basal meltwater supply. Each ice shelf melt tracer is initialized with zero concentration throughout the entire model domain at the beginning of the simulation to track the accumulation of ice shelf meltwater over time. In any model grid cell underneath a floating ice shelf grid point in which melting occurs, the surface flux of tracer into the model is directly proportional to the basal melt rate (set to 0 if there is basal freezing). The tracers advect and diffuse throughout the model domain, providing the temporal and spatial evolution of the distribution of ice shelf meltwater over the continental shelf. Inputs of glacial meltwater derived from iceberg melt or grounded land ice melt that advects to the open ocean through subglacial hydrology (e.g., Death et al., 2014) are not included in the simulation.

The simulated meltwater concentration is related to dFe concentration using a default end member value of 20 nM, which is a conservative number within the range of dFe estimates for glacial meltwater (20–50 nM, Gerringa et al. (2012); 29 ± 21 nM, McGillicuddy et al. (2015); and 22 nM, St-Laurent et al. (2017)). These estimates are based on measurements from meteoric ice (formed from snow),

Table 2
Sources of Dissolved Iron (dFe) Used in the Tracer Simulation

Tracer designation	Tracer source	Tracer location
dFe_{IS1}	Ice shelf melt	Ross Sector
dFe_{IS2}	Ice shelf melt	Amundsen Sector
dFe_{IS3}	Ice shelf melt	Bellingshausen Sector
dFe_{IS4}	Ice shelf melt	Larsen Sector
dFe_{IS5}	Ice shelf melt	Filchner-Ronne Sector
dFe_{IS6}	Ice shelf melt	Queen Maud Sector
dFe_{IS7}	Ice shelf melt	Amery Sector
dFe_{IS8}	Ice shelf melt	Wilkes Sector
dFe_{SED}	Sediments	
dFe_{SED_ZC}	Sediments	Reduced in ice shelf cavities
dFe_{CDW}	Circumpolar Deep Water	
dFe_{CDW_ZC}	Circumpolar Deep Water	Reduced in ice shelf cavities
dFe_{SI}	Sea ice melt	
dFe_{SI_ZC}	Sea ice melt	Reduced in ice shelf cavities

Note. The region included in each sector is shown in Figure 1. Simulations with tracers that are reduced in the ice shelf cavity are indicated by *ZC* (see text for details).

which is the major component of ice shelves, especially in the areas with large basal melt rates. The marine ice (formed from freezing of sea water) at the base of ice shelves is thought to contain significantly more dFe (340–690 nM; Herraiz-Borreguero, Lannuzel, et al., 2016), but the ice shelf dynamics in the circum-Antarctic model do not distinguish between the two ice types. The simulated dFe concentration in a model grid cell is determined by the product of the glacial meltwater fraction and the end member concentration.

Simulation of inputs of dFe from Antarctic continental shelf sediments uses two separate tracers (Table 2). Observational data that allow estimation of the dFe flux from sediments into the bottom shelf waters are lacking and as a result, parameterization of this flux is prone to large uncertainties (Aumont et al., 2015; Tagliabue et al., 2016). However, near-bottom profiles of dFe concentration are available for some Antarctic continental shelf areas that include the Ross Sea (Gerringa et al., 2015; Marsay et al., 2014), the Amundsen Sea (Gerringa et al., 2012; Sherrell et al., 2015), and the west Antarctic Peninsula (Arrigo et al., 2017; Sherrell et al., 2018). Following the approach used in Mack et al. (2017), the dFe concentration in the lowest level of the model was set to a constant value based on the profiles. The bottom concentration of dFe is calculated using the parameterization of St-Laurent et al. (2017), which sets dFe as a function of sea-floor depth at all continental shelf grid points deeper than 300 m and not underneath an ice shelf as:

$$\mathrm{dFe(bottom)} = 0.35\ \mathrm{nM} + (h - 300)\left(\frac{a}{b}\right), \tag{1}$$

where h is the model bottom depth, a (1.7 nM) is the difference between the background dFe concentration at 300 m and the estimated maximum benthic dFe concentration, and b (900 m) is the maximum depth on the shelf minus 300 m. Since the model grid point is one half a vertical grid cell above the bottom of the water column, the value obtained from equation 1 is exponentially reduced based on an empirical equation obtained from measured profiles following St-Laurent et al. (2017):

$$\mathrm{dFe} = \mathrm{dFe(bottom)}e^{-\frac{c}{d}}, \tag{2}$$

where c is the distance (m) from the bottom of the water column to the center of the grid in the lowest vertical level of the model (which is variable due to the terrain following vertical coordinate) and d is a scaling factor (205 m).

The sediment tracer is initialized to 0 everywhere in the model domain and is then nudged to the value obtained from equation 2 in the bottom layer with a time scale of 10 days. The tracer value in the bottom layer of the model is continuously nudged to the estimated sediment concentration throughout the simulation but can freely advect and diffuse throughout the rest of the water column. Note that this is the only tracer where the numerical value carried in the circulation model is in units of dFe (nM).

Two sediment tracers were simulated. The first ($\mathrm{dFe_{SED}}$) is free to advect and diffuse over the entire model domain. The second ($\mathrm{dFe_{SED\_ZC}}$) is restricted within ice shelf cavities. One possible way to explore the effect of the meltwater pump is to run a simulation with ice shelf basal melt turned off. However, the ice shelf basal meltwater has a significant effect on the coastal ocean circulation in some locations. Thus, separating the effects of no meltwater overturning on passive tracers from changes due to active tracers feeding back on the circulation is difficult. St-Laurent et al. (2017) used an approach that relaxed the restricted sediment tracer to 0 with a time scale of 10 days within any ice shelf cavity, which effectively prevents the tracer from exiting the ice shelf cavities without impacting the simulated circulation. This method was adopted for this study. Differences in the unrestricted and restricted sediment tracer distributions in the surface layer over the open continental shelf provide an indication of the effect of ice shelf cavity circulation, including the melt-driven overturning, on the supply of sediment dFe to the euphotic zone around the continent.

The supply of dFe from CDW (Table 2) was simulated in a manner similar to the approach used for sediment dFe. Two CDW tracers are initialized with zero concentration over the entire continental shelf (defined by the 1,200-m isobath and including ice shelf cavities). Off-shelf waters that are defined as CDW (σ_θ [potential density] > 27.6 kg/m^3, potential temperature > 0.0 °C, potential temperature < 2.0 °C, depth below 100 m) are initialized with a tracer value of 1. The off-shelf CDW tracer advects onto the continental shelf below the surface layer and is brought to the surface through vertical mixing and overturning processes. The only source/sink into/out of the model domain of CDW after initialization is well removed from the

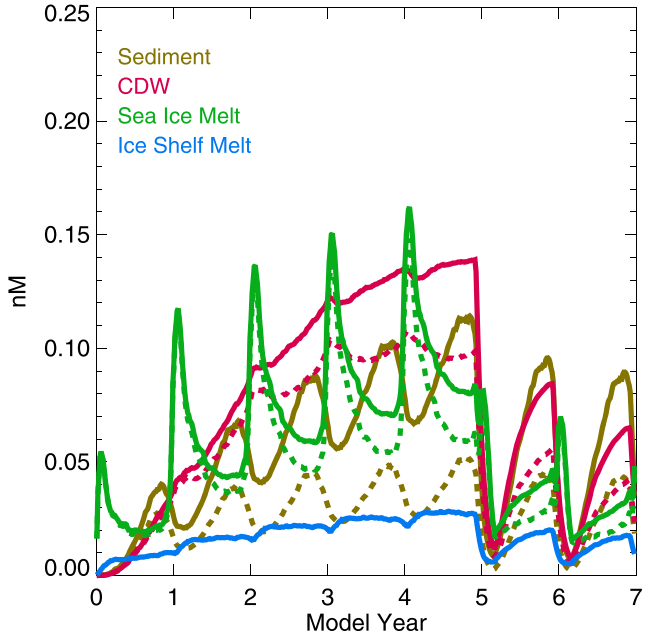

Figure 2. Simulated time evolution of the average surface dFe concentration over the open continental shelf (solid lines) and for tracers set to zero inside ice shelf cavities (dashed lines) obtained for the different sources. Note that biological uptake begins in the summer of year 5/6.

continental shelf at the lateral open boundaries. One CDW tracer (dFe_{CDW}) is free to advect and diffuse over the entire model domain; the second (dFe_{CDW_ZC}) is relaxed to 0 (time scale of 10 days) within any ice shelf cavity. The CDW tracer concentration is related to dFe concentration using a default end member concentration of 0.32 nM, which is an average of measured CDW dFe concentrations just off the Antarctic continental shelf of 0.37 nM (Sherrell et al., 2015) and 0.27 ± 0.5 nM (McGillicuddy et al., 2015).

The supply of dFe from melting sea ice was assessed with two tracers (Table 2). Both sea ice melt tracers are initialized with zero concentration. The surface flux of the sea ice melt tracer into any grid cell is proportional to the melt volume rate of sea ice (set to 0 if there is net freezing of sea water) in that cell. The removal of dFe from the surface water during the growth of sea ice (e.g., Lannuzel et al., 2016) is not included. One sea ice meltwater tracer (dFe_{SI}) advects and diffuses over the entire model domain. The second tracer (dFe_{SI_ZC}) is relaxed to 0 (time scale of 10 days) within any ice shelf cavity. The sea ice melt tracer concentration is related to dFe concentration using a default end member value of 5.0 nM. Lannuzel et al. (2016) show a large range (0.1–110 nM) in measured concentrations of dFe in Antarctic sea ice, and the value of 5.0 nM is consistent with their median value of 4.4 nM.

The different tracers freely advect and diffuse over the model continental shelf for the first 4 years and 11 months of the simulation. In December of the fifth year of simulation, concentrations in the upper part of the water column are reduced to simulate biological uptake. From 1 December through 28 February of the next 2 years of simulation (years 5/6 and 6/7), biological uptake is mimicked by relaxing all tracers to zero in the upper 100 m of the water column with a time scale of 30 days in the upper 50 m and 60 days in the next 50 m of the water column. The final dFe concentrations are directly proportional to the tracer values, which is equivalent to relaxing the dFe concentration to 0 with the same time scale. Although there is evidence in other basins for preferential uptake depending on Fe speciation and origin (Özturk et al., 2003) and for strain-specific uptake of different iron species (Lis et al., 2015; Morel et al., 2008; Rubin et al., 2011), our parameterization of biological uptake effectively consumes the dFe from each source in proportion to its local abundance. We do not account for remineralization, and we assume that all the iron in the model is bound to a ligand and therefore remains in solution in a bioavailable form. Over the same time periods, dFe scavenging, which limits excessive dFe accumulation in the lower portion of the water column, is mimicked by relaxing tracer concentrations throughout the entire water column towards 0 with a time scale of 10^3 days (Dutkiewicz et al., 2005).

3. Model Results

3.1. Surface Layer dFe Supply

The average dFe concentration of the individual tracers over the ice shelf free surface layer of the Antarctic continental shelf generally increases over the first 5 years of the simulation (Figure 2). Using the default values for the different end member concentrations, CDW is the largest contribution (38%, averaged over the last year before "biology" turns on) to the buildup of dFe in the surface waters. Contributions from sea ice melt (28%) and sediments (26%) are similar. Ice shelf melt is a smaller (8%), but not insignificant, component of the overall average. Input of dFe from sea ice melt has a strong seasonal cycle with a summer maximum, as expected. Inputs of sediment dFe are largest in fall and winter during times of stronger vertical mixing over the continental shelf. Contributions to surface dFe from CDW and ice shelf melt are relatively constant. Ice shelf melt does have a seasonal cycle (Figure 6 in Dinniman et al., 2015), but much of this meltwater remains in the ice shelf cavities and is not immediately available to the non-ice shelf covered surface waters of the continental shelf. Therefore, the simulated dFe inputs from this source do not have a pronounced seasonal cycle.

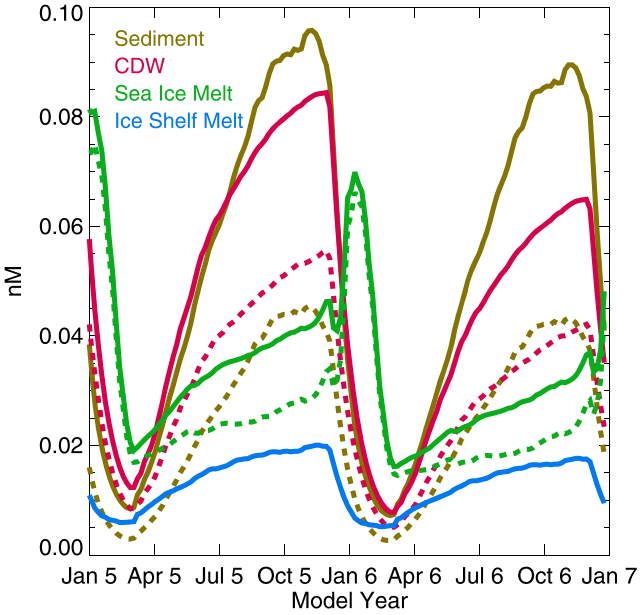

Figure 3. Simulated time evolution of the average surface dFe concentration over the open shelf (solid lines) and for tracers set to 0 inside ice shelf cavities (dashed lines) in the last 2 years of the simulation after biological uptake has been implemented. The full 7-year simulation is shown in Figure 2.

The values of dFe_{SED_ZC} and dFe_{CDW_ZC} become significantly lower than those for dFe_{SED} and dFe_{CDW} over time. This suggests that transport into and out of the ice shelf cavities is, averaged over the entire continental shelf, an important pathway for sediment and CDW sourced dFe into the euphotic zone over the continental shelf. While the spring minima for dFe_{SI_ZC} are somewhat lower than those for dFe_{SI}, the summer maxima are the same every year, indicating that transport into and out of the ice shelf cavities is less important for sea ice derived dFe.

Implementation of biological uptake in the summer of year 5/6 results in drawdown of the surface layer dFe concentrations to almost 0 (Figure 2). The delay in the removal of the dFe from sea ice melt compared to the other sources (Figure 3) results from the competing effect of the supply from summer meltwater and the strength of biological removal. The dFe from sea ice meltwater decreases over the winter during the first 5 years due to vertical mixing of high surface dFe concentrations (only added in summer) with low deeper values. The addition of biological removal reduces the surface dFe concentrations in summer below the deep values, after which there is a small increase over the winter because of vertical mixing that increases the low surface concentrations. The time evolution over the last 2 years of the simulation (Figure 3) shows the resupply of the different dFe sources into the surface layer after the initial summer drawdown, the drawdown to near 0 during the next summer (and early summer supply from sea ice melt), and the subsequent resupply. When summer drawdown is included, sediment (39%, range 30% to 46%; Tables 3 and Supporting Information Table S1) and CDW (32%, range 25% to 34%) sources are the largest suppliers of dFe averaged over the continental shelf surface ocean, while sea ice (23%, range 6% to 47%) and ice shelf melt (6%, range 3% to 14%) are still significant sources.

Restriction of sediment and CDW dFe sources within the ice shelf cavities reduces the contributions of these sources to the non-ice shelf covered surface layer by 52% and 32%, respectively (Figure 3; Table 3). The total dFe concentration is reduced by 32% and by 38% when the direct ice shelf melt contribution is also removed. The restricted sea ice melt contribution of dFe is lower than the unrestricted value during the fall and spring, but maximum values for both are similar in summer (Figure 3).

Table 3
Simulated dFe Supply Averaged Over the Surface Layer of the Open (Not Underneath an Ice Shelf) Antarctic Continental Shelf for the Time Between the Summer Minimum Following Implementation of Biological Drawdown and the Maximum Value Prior to the Start of Summer in the Following Year (or During the Following Summer for Sea Ice Melt)

Symbol (see Table 2)	dFe source	Entire open shelf (nM)	Eastern Amundsen Sea (nM)	Western Ross Sea (nM)
ΣdFe_{ISX}	Ice shelf melt (Sum over all sectors)	0.014	0.045	0.006
dFe_{SED}	Sediments	0.087	0.168	0.122
dFe_{SED_ZC}	Sediments	0.042	0.039	0.081
dFe_{CDW}	Circumpolar Deep Water	0.072	0.046	0.108
dFe_{CDW_ZC}	Circumpolar Deep Water	0.047	0.011	0.090
dFe_{SI}	Sea ice melt	0.051	0.028	0.087
dFe_{SI_ZC}	Sea ice melt	0.049	0.022	0.086
ΣdFe_X	Total supply	0.224	0.287	0.323
$\Sigma dFe_{X\_ZC} + \Sigma dFe_{ISX}$	Total supply without ice shelf cavity contributions	0.153	0.118	0.262
ΣdFe_{X_ZC}	Total supply without ice shelf cavity and ice melt contributions	0.139	0.072	0.256

Note. The dFe concentrations are obtained by scaling the simulated tracer concentrations by the default end member dFe concentrations for each source (see text)

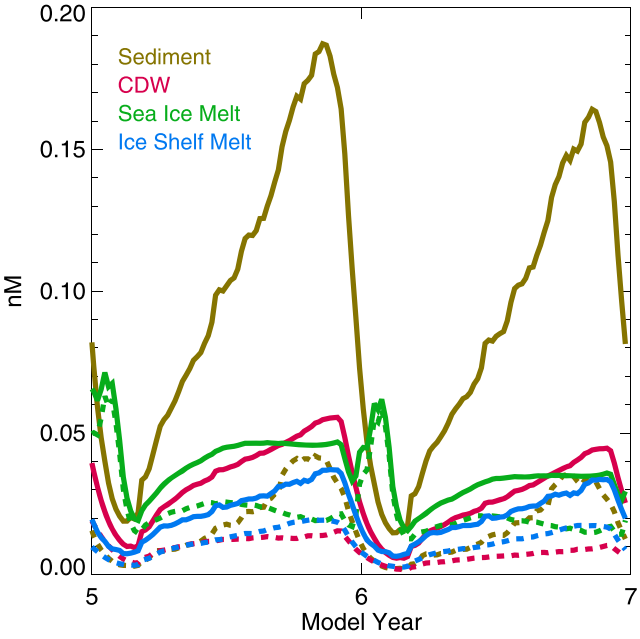

Figure 4. Simulated time evolution of the average surface dFe concentration in the eastern Amundsen Sea (solid lines) and for tracers set to 0 inside ice shelf cavities (dashed lines for sediment, CDW, and sea ice melt) in the last 2 years of the simulation after biological uptake has been implemented. Dashed line for ice shelf melt is all the ice shelf melt that originated outside the Amundsen Sea sector.

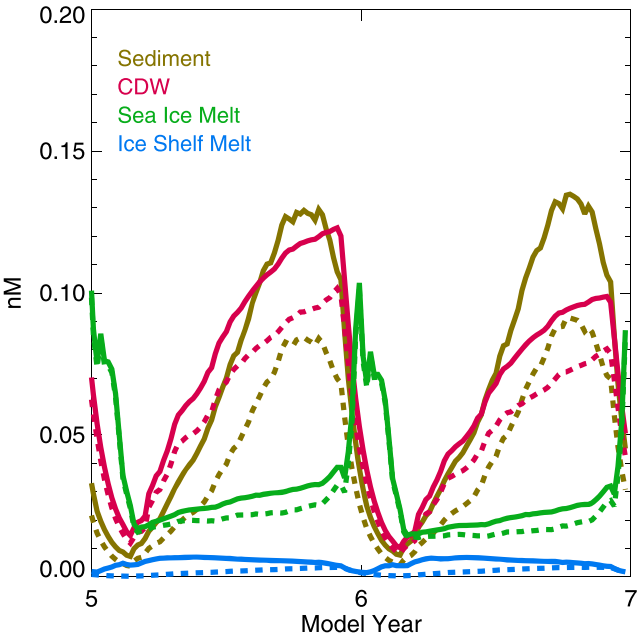

Figure 5. Simulated time evolution of the average surface dFe concentration in the western Ross Sea (solid lines) and for tracers set to 0 inside ice shelf cavities (dashed lines for sediment, CDW, and sea ice melt) in the last 2 years of the simulation after biological uptake has been implemented. Dashed line for ice shelf melt is all the ice shelf melt that originated outside the Ross Sea sector.

The tracer distributions show regional variability. In the eastern Amundsen Sea, both the CDW and sediment tracers first appear on the continental shelf in the deeper part of the water column. This shelf is not characterized by deep vertical mixing (Dutrieux et al., 2014; Heywood et al., 2016; Jacobs et al., 2012) and, as a result, little of the CDW or sediment dFe can reach the surface waters unless it is first transported into an ice shelf cavity (Figure 4). The ice shelf contribution to the surface dFe, whether through direct injection of ice shelf meltwater or meltwater pump-driven overturning of deeper waters within the ice shelf cavities, is 75% of the total modeled supply (Table 3). The model estimate of the total dFe supply to the surface waters before the spring bloom (0.29 nM, Table 3) is similar to the estimate of the winter water mass end member dFe concentration (0.3 ± 0.05 nM) in the Amundsen polynya (Yager et al., 2016).

The simulated inputs of dFe in the western Ross Sea show that the largest contributors to the total surface dFe supply are from the sediment (38%, range 29% to 45%; Figure 5; Tables 3 and S3), CDW (33%, range 26% to 37%), and sea ice (27%, range 7% to 52%) sources. Ice shelf melt is an insignificant contributor, providing only 2% (range 1% to 5%) of the total (Figure 5, Table 3). In contrast to the eastern Amundsen Sea, much of the sediment source (66%) and most of the CDW source (83%) in the western Ross Sea is mixed or upwelled to the surface waters without having to undergo meltwater pump driven overturning within an ice shelf cavity.

The horizontal distribution of the total surface dFe concentration over the Antarctic continental shelf just prior to the second bloom season (Figure 6) shows high dFe concentrations adjacent to ice shelves with low (e.g., Ross ice shelf and Filchner-Ronne ice shelf; Table 1) or high (e.g., Amundsen ice shelves) basal melt rates. The distribution of the ice shelf-related fraction of total dFe supply given by the ratio, (total dFe $-$ ΣdFe_{X_ZC})/Total dFe, shows low values in regions characterized by cold shelf temperatures, deep winter vertical mixing, and low rates of ice shelf melting such as the Ross Sea and much of East Antarctica (Figure 7). Conversely, this fraction is large in areas of the Amundsen and Bellingshausen Seas that are known for warm subsurface shelf temperatures (Schmidtko et al., 2014), reduced vertical mixing, and higher rates of ice shelf basal melt (Figure 7). Over much of the Weddell Sea continental shelf, especially the eastern half, this ratio is greater than 0.5, suggesting that even though the Weddell Sea is considered a "cold" continental shelf, ice shelf processes are important to dFe supply in this region (Figure 7).

3.2. Varying End Member Concentrations

There is considerable variability in observational estimates of the end member concentrations for the different dFe sources, and these ranges were used to assess the effect of end member concentration on the overall dFe supply. The largest range reported here for the ice shelf glacial meltwater dFe source is 29 ± 21 nM (McGillicuddy et al., 2015), which provided minimum and maximum end member estimates for this source of 8 and 50 nM. The mean relative error for the regression of St-Laurent et al. (2017) used to define the bottom concentration of dFe was 33.6%. Therefore, the minimum and maximum dFe estimates used in this study were defined by multiplying the sediment tracer value by 0.66 and 1.34. The minimum and maximum end member concentrations of CDW near

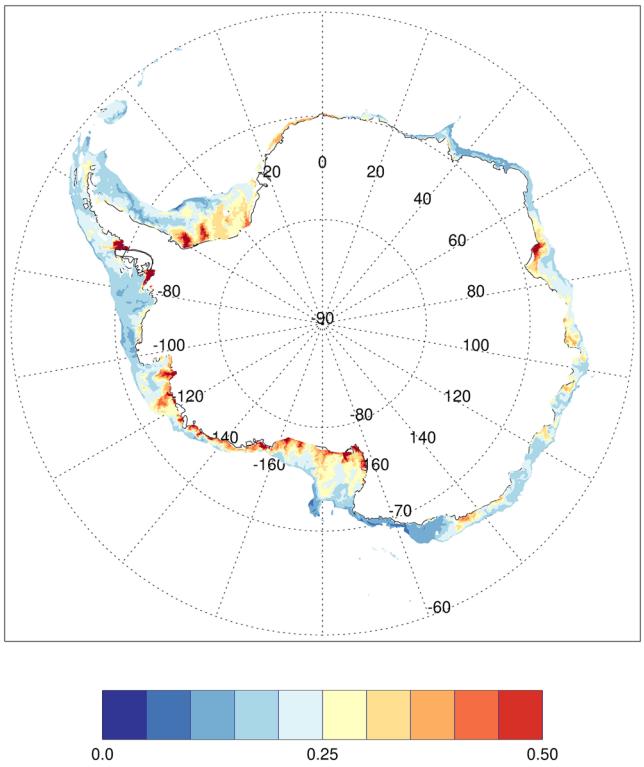

Figure 6. Simulated surface layer total dFe (nM) just prior to the second bloom season (November of simulation year 5).

the Antarctic shelf break were set by direct measurements that ranged from 0.22 nM (McGillicuddy et al., 2015; Sedwick et al., 2011) in Lower CDW (LCDW) off the Ross Sea shelf break to 0.37 nM in Upper CDW (UCDW) off the Amundsen Sea shelf break (Sherrell et al., 2015). Note that the model CDW tracer does not differentiate between LCDW and UCDW. Finally, the measured concentrations of dFe in Antarctic sea ice range from 0.1 to 110 nM, with a median concentration of 4.4 nM (Lannuzel et al., 2016). For this study, a minimum of 1.0 nM (Lannuzel et al., 2010) and a maximum of 15.0 nM (McGillicuddy et al., 2015) were used to specify the dFe range in sea ice. These minimum and maximum end member values for each dFe source tracer were used, along with the previous default best estimate end member values, to examine the range of relative supply of each dFe source (Tables S1–S6).

As mentioned above, the largest contributors to the surface dFe supply, assuming the default end member values, are sediments (39%; Tables 3 and S1) and CDW (32%), with sea ice melt (23%) and ice shelf melt (6%) still being important. Varying the end member concentration of only one component at a time, sediments (30% to 46%, Table S1) and CDW (25% to 35%) maintain their relative contributions to the total supply for any range of end member values, while the contribution from ice shelf melt (3% to 14%) remains smaller but significant. However, the relative contribution from sea ice melt varies widely (6% to 47%) due to the large variance in the end member concentration. Varying all the end member concentrations simultaneously (Table S4) produces increases in the contribution range of each source (sediments: 18% to 64%; CDW: 14% to 53%; ice shelf melt: 2% to 23%; and sea ice melt: 4% to 58%), but the relative contributions of the source terms, other than sea ice melt, remain similar for reasonable ranges of the end member components.

3.3. Comparison With Satellite-Derived Estimates of Chlorophyll and Primary Production

The simulated total surface layer dFe is compared with the satellite-derived estimates of Chl *a* and NPP given in Arrigo et al. (2015). This comparison uses the average Chl *a* estimates from 47 polynyas (the 46 polynyas used in Arrigo et al., 2015 and an additional polynya covering the entire Ross Sea). The simulated dFe for each polynya is the sum of the dFe concentrations from all the nonrestricted tracers (using the default end member values), in the surface layer of the model at the geographical center (as defined in Arrigo et al., 2015) in the spring prior to the second simulated "bloom" (November of year 5).

A linear regression between the estimated Chl *a* and the simulated total dFe (Figure 8a, Table 4) shows a significant correlation (Pearson correlation coefficient $r = 0.477$, two-sided *T*-test probability $p = 7.0 \times 10^{-4}$). However, the high productivity associated with polynyas can result from factors other than dFe availability (Arrigo, 2007; Arrigo et al., 2015), and the availability of dFe is assumed to have a stronger effect at low biomass levels. The calculation was repeated for polynyas with a mean Chl $a < 1.0$ mg m^{-3} ($n = 40$) to test for bias introduced by a few polynyas with high Chl *a* concentrations. The correlation obtained from this regression (Figure 8b) is higher, $r = 0.702$, $p = 4.4 \times 10^{-7}$. A regression using NPP yields similar correlations (Figure S3, Table 4) for all the polynyas ($r = 0.524$) and for the subset ($n = 40$) of polynyas with lower Chl *a* ($r = 0.734$).

Removing the ice shelf cavity contributions (ice shelf melt and tracers that transit inside ice shelf cavities) to the simulated total dFe results in no significant correlation between Chl *a* and simulated total dFe for all the polynyas ($r = 0.204$, $p = 0.168$; Figure 9a, Table 4) and the subset of polynyas with lower mean Chl *a* values ($r = 0.055$, $p = 0.735$; Figure 9b, Table 4). Removing just the ice shelf cavity contribution (while retaining the ice shelf melt) from the total simulated dFe also significantly degraded the correlations (Table 4, $r = 0.362$ or 0.244 [subset of polynyas]). However, removing only the ice shelf melt had little effect on the correlations with Chl *a* (Table 4, $r = 0.477$ or 0.706). There is a similar lack of correlation between NPP and simulated total dFe without ice shelf cavity contributions (Figure S4, Table 4).

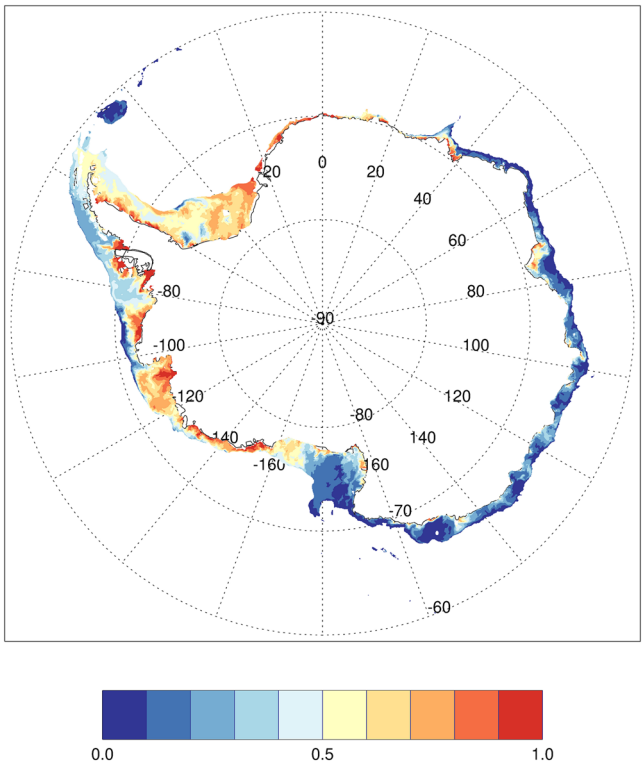

Figure 7. Simulated fraction of ice shelf related dFe to total dFe supply to the surface just prior to the second bloom season (November of simulation year 5).

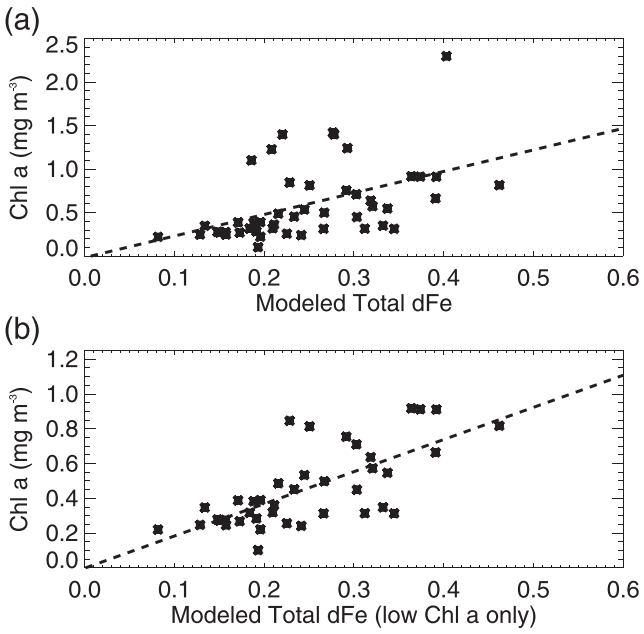

Figure 8. Regression of mean annual chlorophyll a (Chl *a*) concentration against the simulated surface layer total dFe in spring for (a) all coastal polynyas and (b) polynyas with mean Chl $a < 1.0$ mg m^{-3}.

4. Discussion

4.1. Missing dFe Sources

Although the major sources of dFe to surface waters were accounted for in this study, dFe inputs from eolian deposition (Duprat et al., 2019), hydrothermal vents (Ardyna et al., 2019; Tagliabue, 2014; Tagliabue & Resing, 2016), or glacial meltwater from icebergs and the grounded ice sheet were not included. However, these sources are not likely to substantially modify the results obtained from this analysis, with the possible exception of the grounded ice contribution. The dFe inputs from eolian deposition and hydrothermal venting are likely to be insignificant when averaged over the entire Antarctic continental shelf (Boyd et al., 2012; Gao et al., 2013; Lancelot et al., 2009; Tagliabue et al., 2010; Wagener et al., 2008).

Meltwater and sediment delivery from icebergs may be locally important sources of dFe (Duprat et al., 2016; Laufktter et al., 2018; Lin et al., 2011; Raiswell et al., 2008), and a new modeling study suggests that they may be important to dFe delivery over the broader Southern Ocean (Person et al., 2019). However, ice melt from ice shelves is a significant freshwater source to the Antarctic continental shelf (Depoorter et al., 2013; Rignot et al., 2013) and if dFe concentrations in icebergs are similar to those of the floating ice shelves, then ice shelf melt contributions integrated over the continental shelf are more significant than inputs from icebergs (especially since much of the iceberg melt is not over the continental shelf, e.g., Merino et al., 2016).

As mentioned previously, marine ice (formed from freezing of sea water) at the base of ice shelves is thought to contain significantly more dFe (Herraiz-Borreguero, Lannuzel, et al., 2016) than the meteoric ice that makes up most of the Antarctic ice shelves. Thus, marine ice may be an important dFe source near ice shelves where the base of the ice shelf moves so that areas where marine ice is formed are transported away from basal freeze areas to locations where it melts (Herraiz-Borreguero, Church, et al., 2016). However, most of the ice shelf melting around Antarctica is of ice shelves that have very little or no marine ice.

The contribution of dFe from meltwater produced under the grounded ice sheet could be substantial (e.g., Death et al., 2014). However, the quantity of this meltwater that crosses the grounding line, as well as the dFe end member concentration, are subject to large and unknown uncertainties (Death et al., 2014; Hawkings et al., 2014). Particulate iron, which occurs in high concentration in front of some ice shelves (Gerringa et al., 2012; Sherrell et al., 2015), is also not included because it is not thought to be readily bioavailable (Conway et al., 2015; Edwards et al., 2006; Hawkings et al., 2018; Schroth et al., 2009; Spolaor et al., 2013; von der Heyden et al., 2012), although recent work may indicate otherwise (van der Merwe et al., 2019).

4.2. Regional Variability of dFe Supply

Studies of Antarctic polynyas suggest that the sources of dFe that control NPP are variable. For example, the most important sources in the Ross Sea are thought to be sediments and sea ice melt (Mack et al., 2017; McGillicuddy et al., 2015), while sediments and glacial melt dominate in the Amundsen polynya (St-Laurent et al., 2017, 2019), and CDW and sea ice melt are the most important in the Mertz and Ninnis polynyas in

Table 4
Linear Pearson Correlation Coefficients (r) and Two-Sided T-Test Probabilities (p) Obtained From Linear Regressions Between Satellite-Derived Estimates of Chl a and NPP and the Spring Simulated Surface dFe Concentrations for 47 Coastal Polynyas Over the Antarctic Continental Shelf Defined by Arrigo et al. (2015)

Satellite estimate	Dissolved iron sources	*r*	*p*
Chl *a*	Total	**0.477**	7.00×10^{-4}
Chl $a < 1.0$ mg m^{-3}	Total	**0.702**	4.44×10^{-7}
NPP	Total	**0.524**	1.56×10^{-4}
NPP (for Chl $a < 1.0$ mg m^{-3})	Total	**0.734**	6.84×10^{-8}
Chl *a*	Total – ice shelf melt – ice shelf cavity contributions	0.204	0.168
Chl $a < 1.0$ mg m^{-3}	Total – ice shelf melt – ice shelf cavity contributions	0.055	0.735
NPP	Total – ice shelf melt – ice shelf cavity contributions	0.195	0.188
NPP (for Chl $a < 1.0$ mg m^{-3})	Total – ice shelf melt – ice shelf cavity contributions	0.002	0.988
Chl *a*	Total – ice shelf cavity contributions	0.362	0.0123
Chl $a < 1.0$ mg m^{-3}	Total – ice shelf cavity contributions	0.244	0.130
NPP	Total – ice shelf cavity contributions	0.358	0.0133
NPP (for Chl $a < 1.0$ mg m^{-3})	Total – ice shelf cavity contributions	0.190	0.240
Chl *a*	Total – ice shelf melt	**0.477**	6.92×10^{-4}
Chl $a < 1.0$ mg m^{-3}	Total – ice shelf melt	**0.706**	3.64×10^{-7}
NPP	Total – ice shelf melt	**0.526**	1.43×10^{-4}
NPP (for Chl $a < 1.0$ mg m^{-3})	Total – ice shelf melt	**0.735**	6.66×10^{-8}

Note. Significant correlations at the 0.01 level are indicated by bold text. The Total source is the sum of dFe provided by ice shelf melt from all sectors, sediments, CDW, and sea ice melt. The sensitivity of the correlation to removal of the dFe provided by ice shelf melt and the ice shelf cavity is shown. The simulated dFe concentrations were obtained using default end member concentrations (see text).

East Antarctica (Moreau et al., 2019). Correspondingly, the relative importance of the different dFe sources obtained from this simulation shows regional variability. The simulated dFe concentrations in the eastern Amundsen Sea show that sediments contribute most of the surface dFe (48% to 66%, Table S2), independent of end member concentrations. However, in this region, most of the dFe derived from sediments or CDW must be transported into an ice shelf cavity before it is input to surface waters. This result is consistent with the analysis of St-Laurent et al. (2017) for the Amundsen Sea polynya in front of the Dotson Ice Shelf, which showed that the dFe derived from sediments and CDW reaches surface waters via transit through the ice shelf cavity. The strong ice shelf melting in the Amundsen Sea (Depoorter et al., 2013; Jacobs et al., 1996; Liu et al., 2015; Rignot et al., 2013) produces relatively large quantities of ice shelf meltwater (Biddle et al., 2017, 2019; Kim et al., 2016; Randall-Goodwin et al., 2015), and this melting can lead to strong overturning (i.e., meltwater pump) in many of the ice shelf cavities in the region (Jourdain et al., 2017; St-Laurent et al., 2017). As a result, the deep sources of dFe over the entire eastern Amundsen Sea are brought to the surface via a three-dimensional overturning pathway that involves transport at depth into the ice shelf cavity and then transport out of the cavity entrained into a buoyant plume that rises to the surface, rather than via a directly mixed one-dimensional vertical pathway. The simulated estimate of contributions of dFe from ice shelf melt are variable (7% to 32%) but significant. Thus, the total (direct from ice shelf melt and indirect from overturning transport) ice shelf contribution to the surface layer dFe for this region is substantial (57% to 83%). Other dFe sources such as sea ice melt are less important, regardless of end member concentration.

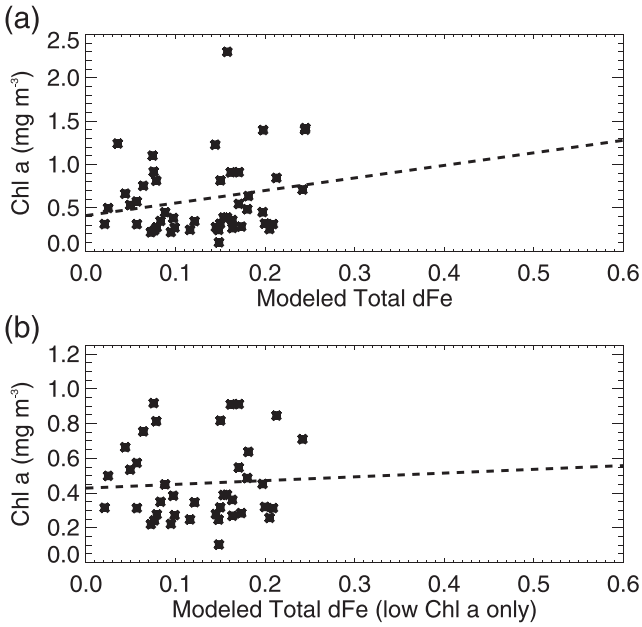

Figure 9. Regression of mean annual chlorophyll *a* (Chl *a*) concentration against the simulated surface layer total dFe (except ice shelf meltwater and ice shelf cavity contributions) in spring for (a) all coastal polynyas and (b) polynyas with mean Chl $a < 1.0$ mg m^{-3}.

The Amundsen Sea polynya is characterized by high Chl *a* concentrations (> 2.0 mg m^{-3}), and the simulated total dFe supply to this region is large (0.4 nM, Figure 8) but is lower than expected from a linear relationship between simulated dFe supply and satellite-derived estimates of Chl *a*.

St-Laurent et al. (2017) implemented a 1.5-km resolution circulation model for this region and found that upstream high melt glaciers, Thwaites and Pine Island, provide dFe to the Amundsen Sea polynya. This additional glacial meltwater source of dFe is underestimated in this study because the 5-km resolution of the circulation model does not resolve a shallow topographic feature that St-Laurent et al. (2017) show affects the along shelf transport. This comparison highlights the need to resolve small-scale bathymetric features as part of estimating controls on NPP in Antarctic continental shelf waters.

In comparison, the western Ross Sea is an area with relatively little ice shelf melt (Depoorter et al., 2013; Jacobs et al., 1992; Liu et al., 2015; Loose et al., 2009; Rignot et al., 2013; Smethie & Jacobs, 2005) but with winter vertical mixing that can extend throughout the entire water column in some locations (Gordon et al., 2000; Manzella et al., 1999; Piñones et al., 2019). The simulated tracer distribution in the western Ross Sea indicates that ice shelf melt is a small contributor (1% to 5%, Table S3) to surface dFe for all end member concentration estimates. As opposed to the eastern Amundsen Sea, much of the sediment source (66%) and most of the CDW source (83%) of dFe in the western Ross Sea are brought to the surface through one-dimensional vertical mixing without having to go through the Ross ice shelf cavity (e.g., the discussion of a "winter reserve" in McGillicuddy et al., 2015). Depending on the end member value used, either sediments (maximum of 45% of the total) or sea ice melt (maximum of 52%) is the largest contributor to surface dFe, and CDW (26% to 37%) remains important. This is consistent with iron budget analyses using a regional circulation model for the Ross Sea (Mack et al., 2017; McGillicuddy et al., 2015). The estimate of the total dFe supply to the surface waters of the western Ross Sea before the spring bloom (0.32 nM) obtained in this study is similar to the McGillicuddy et al. (2015) estimate of the "winter reserve" dFe (0.29 ± 0.11 nM) in the same area.

The Weddell Sea is another region with cold shelf temperatures and deep winter vertical mixing (Foldvik et al., 1985; Nicholls et al., 2009) with relatively small ice shelf melt from the adjacent Filchner-Ronne Ice Shelf (Nicholls et al., 2009; Rignot et al., 2013; Depoorter et al., 2013; Liu et al., 2015). Hence, the expectation for surface dFe inputs is for minimal effect from ice shelf melt or water that was transported through the adjacent ice shelf cavity. However, the Riiser-Larsen and Fimbul ice shelves to the east of the Weddell Sea continental shelf have significant ice melt and cover most of the continental shelf in those areas (Hattermann et al., 2012; Nøst, 2004). As a result, most of the shelf circulation of these regions transits underneath the ice shelf. The circulation along the slope and shelf is from the east into the Weddell Sea (Fahrbach et al., 1994; Nicholls et al., 2009) and has a strong effect on water properties in the Weddell Sea (Graham et al., 2013). This advective input to the Weddell Sea from upstream represents a significant source of dFe to the surface layer from water that was in an ice shelf cavity but not necessarily the adjacent Filchner-Ronne ice shelf.

4.3. Polynya Primary Production and Ice Shelves

The correlation between the satellite-derived estimates of Chl *a* (or the NPP) and the simulated total dFe over all polynyas supports the hypothesis that NPP in the coastal polynyas is limited by dFe availability in the surface waters. Variability in this correlation is from regional differences in the strength of the dFe supply. Removing the ice shelf cavity contributions to the simulated total dFe removes any significant correlation between the simulated total dFe and satellite Chl *a* or NPP. The productivity of the coastal polynyas therefore does appear to be related to the basal melt of adjacent ice shelves as found in Arrigo et al. (2015). However, rather than being directly influenced by the release of dFe from melting ice shelves, the much larger impact appears to be circulation changes driven by ice shelf melt that allow other, deeper, sources of dFe to be advected or mixed into the upper well-lit waters over the continental shelf.

5. Conclusions

This study shows that direct injection of iron from melting ice can be an important contributor to the total dFe supply to the surface waters in some locations. However, there is generally a much larger contribution from deep sources of iron on the shelf. The contribution of dFe supply from the basal melt driven overturning circulation within ice shelf cavities is heterogeneous around Antarctica, but in several locations, this meltwater pump is the primary mechanism for transporting deep dFe up to the surface.

The sources of dFe to Antarctic surface waters are heterogeneous. If dFe remains a primary limiting factor for phytoplankton growth, this heterogeneity makes predicting future changes in NPP a complex problem with different drivers around the continent. For example, if current trends in the warming of Amundsen Sea shelf waters (Schmidtko et al., 2014) and increasing melt of Amundsen sector ice shelves (Paolo et al., 2015) continue as projected (Naughten et al., 2018), then the expectation is an increased meltwater pump, possibly leading to more surface dFe availability in the Amundsen Sea. However, increased Amundsen ice shelf melt has been implicated in the observed freshening in the downstream Ross Sea (Jacobs et al., 2002; Jacobs & Giulivi, 2010; Nakayama et al., 2014), which may lead to reduced vertical mixing of deep water masses on the continental shelf without much of a change in ice shelf basal melt (Dinniman et al., 2018), and thus reduced surface dFe supply in the Ross Sea.

Projections of ice shelf basal melt have large uncertainties due to many factors, including a sensitivity to variability in the atmospheric forcing (e.g., Timmermann & Hellmer, 2013). However, projections for the next 100 years suggest a relatively great increase in basal melt in the Amundsen, Bellingshausen, and eastern Weddell Sea ice shelves compared to the rest of the continent (Figure 3 in Naughten et al., 2018). The simulations from this study indicate that these regions are currently important with respect to ice shelf melt control of dFe supply. Enhanced nutrient supply in these regions may result in increased phytoplankton productivity in the adjacent polynyas. Increased primary production, and any changes in the surface phytoplankton species composition due to a relaxation of dFe limitation (e.g., Zhu et al., 2016), will have important consequences for higher trophic level organisms that rely on phytoplankton for a food source, potentially leading to a restructuring of the interconnected food web around the Antarctic continent. Thus, the numerous polynyas surrounding the Antarctic continent need to be treated as an interconnected system exchanging physical, chemical, and biological properties, an undertaking best achieved using a mechanistic modeling approach.

Acknowledgments
This research was supported by the National Science Foundation under grants OPP-1643652 to Old Dominion University and OPP-1643618 to Stanford University, and by the Turing High Performance Computing cluster at Old Dominion University. We thank P. Yager and R. Sherrell for very helpful discussions. Comments from two anonymous reviewers considerably improved the manuscript. The circulation model data (including all simulated dyes) used for this analysis are available at BCO-DMO at https://www.bco-dmo.org/dataset/782848.

References

Adler, R. F., Huffman, G. J., Chang, A., Ferraro, R., Xie, P. P., Janowiak, J., et al. (2003). The version 2 global precipitation climatology project (GPCP) monthly precipitation analysis (1979–present). *Journal of Hydrometeorology*, *4*, 1147–1167. https://doi.org/10.1175/1525-7541(2003)004,1147:TVGPCP.2.0.CO;2

Adusumilli, S., Fricker, H. A., Siegfried, M. R., Padman, L., Paolo, F. S., & Ligtenberg, S. R. M. (2018). Variable basal melt rates of Antarctic Peninsula ice shelves, 1994–2016. *Geophysical Research Letters*, *45*, 4086–4095. https://doi.org/10.1002/2017GL076652

Ardyna, M., Lacour, L., Sergi, S., d'Ovidio, F., Sallée, J. B., Rembauville, M., et al. (2019). Hydrothermal vents trigger massive phytoplankton blooms in the Southern Ocean. *Nature Communications*, *10*(1), 1–8. https://doi.org/10.1038/s41467-019-09973-6

Arrigo, K. R. (2007). Physical control of primary production in Arctic and Antarctic polynyas. In W. O. Smith, & D. G. Barber (Eds.), *Polynyas: Windows to the world*, *Elsevier Oceanography Series*, (Vol. 74, pp. 223–238). Amsterdam, The Netherlands: Elsevier. https://doi.org/10.1016/S0422-9894(06)74007-7

Arrigo, K. R., DiTullio, G. R., Dunbar, R. B., Robinson, D. H., VanWoert, M., Worthen, D. L., & Lizotte, M. P. (2000). Phytoplankton taxonomic variability and nutrient utilization and primary production in the Ross Sea. *Journal of Geophysical Research*, *105*, 8827–8846.

Arrigo, K. R., & van Dijken, G. L. (2003). Phytoplankton dynamics within 37 Antarctic coastal polynyas. *Journal of Geophysical Research*, *108*(C8), 3271. https://doi.org/10.1029/2002JC001739

Arrigo, K. R., van Dijken, G. L., Alderkamp, A.-C., Erickson, Z. K., Lewis, K. M., Lowry, K. E., et al. (2017). Early spring phytoplankton dynamics in the western Antarctic pPeninsula. *Journal of Geophysical Research: Oceans*, *122*, 9350–9369. https://doi.org/10.1002/2017JC013281

Arrigo, K. R., van Dijken, G. L., & Bushinsky, S. (2008). Primary production in the Southern Ocean, 1997–2006. *Journal of Geophysical Research*, *113*, C08004. https://doi.org/10.1029/2007JC004551

Arrigo, K. R., van Dijken, G. L., & Long, M. C. (2008). The coastal Southern Ocean: A strong anthropogenic CO_2 sink. *Geophysical Research Letters*, *35*, L21602. https://doi.org/10.1029/2008GL035624

Arrigo, K. R., van Dijken, G. L., & Strong, A. L. (2015). Environmental controls of marine productivity hot spots around Antarctica. *Journal of Geophysical Research: Oceans*, *120*, 5545–5565. https://doi.org/10.1002/2015JC010888

Arrigo, K. R., Worthen, D. L., Schnell, A., & Lizotte, M. P. (1998). Primary production in Southern Ocean waters. *Journal of Geophysical Research*, *103*, 15,587–15,600.

Aumont, O., Ethé, C., Tagliabue, A., Bopp, L., & Gehlen, M. (2015). PISCES-v2: An ocean biogeochemical model for carbon and ecosystem studies. *Geoscientific Model Development*, *8*, 465–2513. https://doi.org/10.5194/gmd-8-2465-2015

Biddle, L., Heywood, K., Kaiser, J., & Jenkins, A. (2017). Glacial meltwater identification in the Amundsen Sea. *Journal of Physical Oceanography*, *47*, 933–954. https://doi.org/10.1175/JPO-D-16-0221.1

Biddle, L. C., Loose, B., & Heywood, K. J. (2019). Upper ocean distribution of glacial meltwater in the Amundsen Sea, Antarctica. *Journal of Geophysical Research: Oceans*, *124*, 6854–6870. https://doi.org/10.1002/2019JC015133

Boyd, P. W. (2002). Environmental factors controlling phytoplankton processes in the Southern Ocean. *Journal of Phycology*, *38*, 844–861. https://doi.org/10.1046/j.1529-8817.2002.t01-1-01203.x

Boyd, P. W., Arrigo, K. R., Strzepek, R., & van Dijken, G. L. (2012). Mapping phytoplankton iron utilization: Insights into Southern Ocean supply mechanisms. *Journal of Geophysical Research*, *117*, C06009. https://doi.org/10.1029/2011JC007726

Budgell, P. (2005). Numerical simulation of ice-ocean variability in the Barents Sea region towards dynamical downscaling. *Ocean Dynamics*, *55*, 370–387.

Comiso, J. C. (2010). *Polar oceans from space*, (p. 507). New York: Springer.
Conway, T. M., Wolff, E. W., Röthlisberger, R., Mulvaney, R., & Elderfield, H. E. (2015). Constraints on soluble aerosol iron flux to the Southern Ocean at the last glacial maximum. *Nature Communications*, *6*, 7850. https://doi.org/10.1038/ncomms8850
Corr, H. F. J., Jenkins, A., Nicholls, K. W., & Doake, C. S. M. (2002). Precise measurement of changes in ice-shelf thickness by phase-sensitive radar to determine basal melt rates. *Geophysical Research Letters*, *29*(8), 1226. https://doi.org/10.1029/2001GL014606
De Baar, H. J. W., Buma, A. G. J., Nolting, R. F., Cadee, G. C., Jacques, G., & Treguer, P. J. (1990). On iron limitation of the Southern Ocean: Experimental observations in the Weddell and Scotia Sea. *Marine Ecology Progress Series*, *65*, 105–122.
Death, R., Wadham, J. L., Monteiro, F., Le Brocq, A. M., Tranter, M., Ridgwell, A., et al. (2014). Antarctic ice sheet fertilises the Southern Ocean. *Biogeosciences*, *11*, 2635–2644. https://doi.org/10.5194/bg-11-2635-2014
Dee, D. P., Uppala, S. M., Simmons, A. J., Berrisford, P., Poli, P., Kobayashi, S., et al. (2011). The ERA-Interim reanalysis: Configuration and performance of the data assimilation system. *Quarterly Journal of the Royal Meteorological Society*, *137*, 553–597. https://doi.org/10.1002/qj.828
Depoorter, M. A., Bamber, J. L., Griggs, J. A., Lenaerts, J. T. M., Ligtenberg, S. R. M., van den Broeke, M. R., & Moholdt, G. (2013). Calving fluxes and basal melt rates of Antarctic ice shelves. *Nature*. https://doi.org/10.1038/nature12567
Dinniman, M. S., Asay-Davis, X. S., Galton-Fenzi, B. K., Holland, P. R., Jenkins, A., & Timmermann, R. (2016). Modeling ice shelf/ocean interaction in Antarctica: A review. *Oceanography*, *29*(4), 144–153. https://doi.org/10.5670/oceanog.2016.106
Dinniman, M. S., Klinck, J. M., Bai, L.-S., Bromwich, D. H., Hines, K. M., & Holland, D. M. (2015). The effect of atmospheric forcing resolution on delivery of ocean heat to the Antarctic floating ice shelves. *Journal of Climate*, *28*, 6067–6085. https://doi.org/10.1175/JCLI-D-14-00374.1
Dinniman, M. S., Klinck, J. M., & Hofmann, E. E. (2012). Sensitivity of circumpolar deep water transport and ice shelf basal melt along the West Antarctic Peninsula to changes in the winds. *Journal of Climate*, *25*, 4799–4816. https://doi.org/10.1175/JCLI-D-11-00307.1
Dinniman, M. S., Klinck, J. M., Hofmann, E. E., & Smith, W. O. Jr. (2018). Effects of projected changes in wind, atmospheric temperature, and freshwater inflow on the Ross Sea. *Journal of Climate*, *31*, 1619–1635. https://doi.org/10.1175/JCLI-D-17-0351.1
Dinniman, M. S., Klinck, J. M., & Smith, W. O. Jr. (2011). A model study of Circumpolar Deep Water on the West Antarctic Peninsula and Ross Sea continental shelves. *Deep Sea Research, Part II*, *58*, 1508–1523. https://doi.org/10.1016/j.dsr2.2010.11.013
Duprat, L., Kanna, N., Janssens, J., Roukaerts, A., Deman, F., Townsend, A. T., et al. (2019). Enhanced iron flux to Antarctic sea ice via dust deposition from ice-free coastal areas. *Journal of Geophysical Research: Oceans*, *124*, 8538–8557. https://doi.org/10.1029/2019JC015221
Duprat, L. P. A. M., Bigg, G. R., & Wilton, D. J. (2016). Enhanced Southern Ocean marine productivity due to fertilization by giant icebergs. *Nature Geoscience*, *9*, 219–221. https://doi.org/10.1038/NGEO2633
Dutkiewicz, S., Follows, M. J., & Parekh, P. (2005). Interactions of the iron and phosphorus cycles: A three-dimensional model study. *Global Biogeochemical Cycles*, *19*, GB1021. https://doi.org/10.1029/2004GB002342
Dutrieux, P., De Rydt, J., Jenkins, A., Holland, P. R., Ha, H. K., Lee, S. H., et al. (2014). Strong sensitivity of Pine Island ice-shelf melting to climatic variability. *Science*, *343*(6167), 174–178. https://doi.org/10.1126/science.1244341
Edwards, R., Sedwick, P., Morgan, V., & Boutron, C. (2006). Iron in ice cores from Law Dome: A record of atmospheric iron deposition for maritime East Antarctica during the Holocene and Last Glacial Maximum. *Geochemistry, Geophysics, Geosystems*, *7*, Q12Q01. https://doi.org/10.1029/2006GC001307
Fahrbach, E., Peterson, R. G., Rohardt, G., Schlosser, P., & Bayer, R. (1994). Suppression of bottom water formation in the southeastern Weddell Sea. *Deep Sea Research, Part I*, *41*, 389–411.
Fairall, C. W., Bradley, E. F., Hare, J. E., Grachev, A. A., & Edson, J. B. (2003). Bulk parameterization of air-sea fluxes: Updates and verification for the COARE algorithm. *Journal of Climate*, *16*, 571–591.
Fitzwater, S. E., Johnson, K. S., Gordon, R. M., Coale, K. H., & Smith, W. O. (2000). Trace metal concentrations in the Ross Sea and their relationship with nutrients and phytoplankton growth. *Deep-Sea Research Part II*, *47*, 3159–3179. https://doi.org/10.1016/S0967-0645(00)00063-1
Foldvik, A., Gammelsrød, T., & Tørresen, T. (1985). Circulation and water masses on the southern Weddell Sea shelf. Circulation and water masses on the southern Weddell Sea shelf. In S. S. Jacobs (Ed.), *Oceanology of the Antarctic Continental Shelf*, *AGU Antarctic Research Series*, (Vol. 43, pp. 5–20). Washington, DC: American Geophysical Union.
Gao, Y., Xu, G., Zhan, J., Zhang, J., Li, W., Lin, Q., et al. (2013). Spatial and particle size distributions of atmospheric dissolvable iron in aerosols and its input to the Southern Ocean and coastal East Antarctica. *Journal of Geophysical Research: Oceans*, *118*, 12,634–12,648. https://doi.org/10.1002/2013JD020367
Gerringa, L. J. A., Alderkamp, A., Laan, P., Thuróczy, C., De Baar, H. J. W., Mills, M. M., et al. (2012). Iron from melting glaciers fuels the phytoplankton blooms in Amundsen Sea (Southern Ocean): Iron biogeochemistry. *Deep Sea Research, Part II*, *71–76*, 16–31. https://doi.org/10.1016/j.dsr2.2012.03.007
Gerringa, L. J. A., Laan, P., van Dijken, G. L., van Haren, H., De Baar, H. J. W., Arrigo, K. R., & Alderkamp, A.-C. (2015). Sources of iron in the Ross Sea polynya in late spring and summer. *Marine Chemistry*, *177*, 447–459. https://doi.org/10.1016/j.marchem.2015.06.002
Gledhill, M., & Buck, K. N. (2012). The organic complexation of iron in the marine environment: A review. *Frontiers in Microbiology*, *3*, 69. https://doi.org/10.3389/fmicb.2012.00069
Gordon, L. I., Codispoti, L. A., Jennings, J. C. Jr., Millero, F. J., Morrison, J. M., & Sweeney, C. (2000). Seasonal evolution of hydrographic properties in the Ross Sea, Antarctica, 1996-1997. *Deep Sea Research, Part II*, *47*, 3095–3117. https://doi.org/10.1016/S0967-0645(00)00060-6
Graham, J. A., Dinniman, M. S., & Klinck, J. M. (2016). Impact of model resolution for on-shelf heat transport along the West Antarctic Peninsula. *Journal of Geophysical Research: Oceans*, *121*, 7880–7897. https://doi.org/10.1002/2016JC011875
Graham, J. A., Heywood, K. J., Chavanne, C. P., & Holland, P. R. (2013). Seasonal variability of water masses and transport on the Antarctic continental shelf and slope in the southeastern Weddell Sea. *Journal of Geophysical Research: Oceans*, *118*, 2201–2214. https://doi.org/10.1002/jgrc.20174
Greisman, P. (1979). On upwelling driven by the melt of ice shelves and tidewater glaciers. *Deep Sea Res. A*, *26A*, 1051–1065.
Haidvogel, D. B., Arango, H., Budgell, W. P., Cornuelle, B. D., Curchitser, E., Di Lorenzo, E., et al. (2008). Ocean forecasting in terrain-following coordinates: Formulation and skill assessment of the Regional Ocean Modeling System. *Journal of Computational Physics*, *227*, 3595–3624. https://doi.org/10.1016/j.jcp.2007.06.016
Häkkinen, S., & Mellor, G. L. (1992). Modeling the seasonal variability of a coupled Arctic ice-ocean system. *Journal of Geophysical Research*, *97*, 20,285–20,304.

Hattermann, T., Nøst, O. A., Lilly, J. M., & Smedsrud, L. H. (2012). Two years of oceanic observations below the Fimbul ice shelf, Antarctica. *Geophysical Research Letters*, *39*, L12605. https://doi.org/10.1029/2012GL051012

Hawkings, J. R., Benning, L. G., Raiswell, R., Kaulich, B., Araki, T., Abyaneh, M., et al. (2018). Biolabile ferrous iron bearing nanoparticles in glacial sediments. *Earth and Planetary Science Letters*, *493*, 92–101. https://doi.org/10.1016/j.epsl.2018.04.022

Hawkings, J. R., Wadham, J. L., Tranter, M., Raiswell, R., Benning, L. G., Statham, P. J., et al. (2014). Ice sheets as a significant source of highly reactive nanoparticulate iron to the oceans. *Nature Communications*, *5*, 3929. https://doi.org/10.1038/ncomms4929

Herraiz-Borreguero, L., Church, J. A., Allison, I., Peña-Molino, B., Coleman, R., Tomczak, M., & Craven, M. (2016). Basal melt, seasonal water mass transformation, ocean current variability, and deep convection processes along the Amery ice shelf calving front, East Antarctica. *Journal of Geophysical Research: Oceans*, *121*, 4946–4965. https://doi.org/10.1002/2016JC011858

Herraiz-Borreguero, L., Lannuzel, D., van der Merwe, P., Treverrow, A., & Pedro, J. B. (2016). Large flux of iron from the Amery ice shelf marine ice to Prydz Bay, East Antarctica. *Journal of Geophysical Research: Oceans*, *121*, 6009–6020. https://doi.org/10.1002/2016JC011687

Heywood, K. J., Biddle, L. C., Boehme, L., Dutrieux, P., Fedak, M., Jenkins, A., et al. (2016). Between the devil and the deep blue sea: The role of the Amundsen Sea continental shelf in exchanges between ocean and ice shelves. *Oceanography*, *29*, 118–129. https://doi.org/10.5670/oceanog.2016.104

Holland, D. M., & Jenkins, A. (1999). Modelling thermodynamic ice-ocean interactions at the base of an ice shelf. *Journal of Physical Oceanography*, *29*, 1787–1800.

Hunke, E. C. (2001). Viscous-plastic sea ice dynamics with the EVP model: Linearization issues. *Journal of Computational Physics*, *170*, 18–38.

Hunke, E. C., & Dukowicz, J. K. (1997). An elastic-viscous-plastic model for sea ice dynamics. *Journal of Physical Oceanography*, *27*, 1849–1867.

Jacobs, S., Giulivi, C., Dutrieux, P., Rignot, E., Nitsche, F., & Mouginot, J. (2013). Getz ice shelf melting response to changes in ocean forcing. *Journal of Geophysical Research: Oceans*, *118*, 4152–4168. https://doi.org/10.1002/jgrc.20298

Jacobs, S., Jenkins, A., Hellmer, H., Giulivi, C., Nitsche, F., Huber, B., & Guerrero, R. (2012). The Amundsen Sea and the Antarctic ice sheet. *Oceanography*, *25*(3), 154–163. https://doi.org/10.5670/oceanog.2012.90

Jacobs, S. S., & Giulivi, C. F. (2010). Large multidecadal salinity trends near the Pacific-Antarctic continental margin. *Journal of Climate*, *23*, 4508–4524. https://doi.org/10.1175/2010JCLI3284.1

Jacobs, S. S., Giulivi, C. F., & Mele, P. A. (2002). Freshening of the Ross Sea during the late 20th century. *Science*, *297*(5580), 386–389. https://doi.org/10.1126/science.1069574

Jacobs, S. S., Hellmer, H. H., Doake, C. S. M., Jenkins, A., & Frolich, R. (1992). Melting of ice shelves and the mass balance of Antarctica. *Journal of Glaciology*, *38*, 375–387.

Jacobs, S. S., Hellmer, H. H., & Jenkins, A. (1996). Antarctic ice sheet melting in the Southeast Pacific. *Geophysical Research Letters*, *23*, 957–960.

Jacobs, S. S., Jenkins, A., Giulivi, C. F., & Dutrieux, P. (2011). Stronger ocean circulation and increased melting under Pine Island glacier ice shelf. *Nature Geoscience*, *4*, 519–523. https://doi.org/10.1038/ngeo1188

Jenkins, A., & Jacobs, S. S. (2008). Circulation and melting beneath George VI ice shelf, Antarctica. *Journal of Geophysical Research*, *113*, C04013. https://doi.org/10.1029/2007JC004449

Jourdain, N. C., Mathiot, P., Merino, N., Durand, G., Le Sommer, J., Spence, P., et al. (2017). Ocean circulation and sea-ice thinning induced by melting ice shelves in the Amundsen Sea. *Journal of Geophysical Research: Oceans*, *122*, 2550–2573. https://doi.org/10.1002/2016JC012509

Karnovsky, N., Ainley, D. G., & Lee, P. (2007). The impact and importance of production in Polynyas to top-trophic predators: Three case histories. In W. O. Smith, & D. G. Barber (Eds.), *Polynyas: Windows to the world*, *Elsevier Oceanography Series*, (Vol. 74, pp. 391–410). Amsterdam, The Netherlands: Elsevier.https://doi.org/10.1016/S0422-9894(06)74012-0

Kim, I., Hahm, D., Rhee, T. S., Kim, T. W., Kim, C. S., & Lee, S. (2016). The distribution of glacial meltwater in the Amundsen Sea, Antarctica, revealed by dissolved helium and neon. *Journal of Geophysical Research: Oceans*, *121*, 1654–1666. https://doi.org/10.1002/2015JC011211

Lancelot, C., de Montety, A., Goosse, H., Becquevort, S., Schoemann, V., Pasquer, B., & Vancoppenolle, M. (2009). Spatial distribution of the iron supply to phytoplankton in the Southern Ocean: A model study. *Biogeosciences*, *6*, 2861–2878. https://doi.org/10.5194/bg-6-2861-2009

Langley, K., Kohler, J., Sinisalo, A., Øyan, M. J., Hamran, S. E., Hattermann, T., et al. (2014). Low melt rates with seasonal variability at the base of Fimbul ice shelf, East Antarctica, revealed by in situ interferometric radar measurements. *Geophysical Research Letters*, *41*. https://doi.org/10.1002/2014GL061782

Lannuzel, D., Schoemann, V., de Jong, J., Paswuer, B., van der Merwe, P., Masson, F., et al. (2010). Distribution of dissolved iron in Antarctic sea ice: Spatial, seasonal, and inter-annual variability. *Journal of Geophysical Research*, *115*, G03022. https://doi.org/10.1029/2009JG001031

Lannuzel, D., Vancoppenolle, M., van der Merwe, P., de Jong, J., Meiners, K. M., Grotti, M., et al. (2016). Iron in sea ice: Review and new insights. *Elementa: Science of the Anthropocene*, *4*(000130), 130. https://doi.org/10.12952/journal.elementa.000130

Large, W. G., McWilliams, J. C., & Doney, S. C. (1994). Oceanic vertical mixing: A review and a model with nonlocal boundary layer parameterization. *Reviews of Geophysics*, *32*, 363–403. https://doi.org/10.1029/94RG01872

Laufktter, C., Stern, A. A., John, J. G., Stock, C. A., & Dunne, J. P. (2018). Glacial iron sources stimulate the Southern Ocean carbon cycle. *Geophysical Research Letters*, *45*, 13,377–13,385. https://doi.org/10.1029/2018GL079797

Lin, H., Rauschenberg, S., Hexel, C. R., Shaw, T. J., & Twining, B. S. (2011). Free-drifting icebergs as sources of iron to the Weddell Sea. *Deep Sea Research, Part II*, *58*, 1392–1406. https://doi.org/10.1016/j.dsr2.2010.11.020

Lis, H., Kranzler, C., Keren, N., & Shaked, Y. (2015). A comparative study of iron uptake rates and mechanisms amongst marine and fresh water cyanobacteria: Prevalence of reductive iron uptake. *Lifestyles*, *5*, 841–860. https://doi.org/10.3390/life5010841

Liu, Y., Moore, J. C., Cheng, X., Gladstone, R. M., Bassis, J. N., Liu, H., et al. (2015). Ocean-driven thinning enhances iceberg calving and retreat of Antarctic ice shelves. *Proceedings of the National Academy of Sciences*, *112*(11), 3263–3268. https://doi.org/10.1073/pnas.1415137112

Loose, B., Schlosser, P., Smethie, W. M., & Jacobs, S. (2009). An optimized estimate of glacial melt from the Ross ice shelf using noble gases, stable isotopes, and CFC transient tracers. *Journal of Geophysical Research*, *114*, C08007. https://doi.org/10.1029/2008JC005048

Mack, S. L., Dinniman, M. S., McGillicuddy, D. J. Jr., Sedwick, P. N., & Klinck, J. M. (2017). Dissolved iron transport pathways in the Ross Sea: Influence of tides and mesoscale eddies in a regional ocean model. *Journal of Marine Systems*, *166*, 73–86. https://doi.org/10.1016/j.marsys.2016.10.008

Mahowald, N. M., Engelstaedter, S., Luo, C., Sealy, A., Artaxo, P., Benitez-Nelson, C., et al. (2009). Atmospheric iron deposition: Global distribution, variability, and human perturbations. *Annual Review of Marine Science*, *1*, 245–278.
Manzella, G. M. R., Meloni, R., & Picco, P. (1999). Current, temperature and salinity observations in the Terra Nova Bay Polynya area. In G. Spezie, & G. M. R. Manzella (Eds.), *Oceanography of the Ross Sea, Antarctica*, (pp. 165–173). New York: Springer.
Marsay, C. M., Sedwick, P. N., Dinniman, M. S., Barrett, P. M., Mack, S. L., & McGillicuddy, D. J. (2014). Estimating the benthic efflux of dissolved iron on the Ross Sea continental shelf. *Geophysical Research Letters*, *41*, 7576–7583. https://doi.org/10.1002/2014GL061684
Martin, J. H., Fitzwater, S. E., & Gordon, R. M. (1990). Iron deficiency limits plankton growth in Antarctic waters. *Global Biogeochemical Cycles*, *4*, 5–12.
McGillicuddy, D. J., Sedwick, P. N., Dinniman, M. S., Arrigo, K. R., Bibby, T. S., Greenan, B. J. W., et al. (2015). Iron supply and demand in an Antarctic shelf ecosystem. *Geophysical Research Letters*, *42*, 8088–8097. https://doi.org/10.1002/2015GL065727
Mellor, G. L., & Kantha, L. (1989). An ice-ocean coupled model. *Journal of Geophysical Research*, *94*, 10,937–10,954.
Merino, N., Le Sommer, J., Durand, G., Jourdain, N. C., Madec, G., Mathiot, P., & Tournadre, J. (2016). Antarctic icebergs melt over the Southern Ocean: Climatology and impact on sea ice. *Ocean Modelling*, *104*, 99–110. https://doi.org/10.1016/j.ocemod.2016.05.001
Millan, R., Rignot, E., Bernier, V., Morlighem, M., & Dutrieux, P. (2017). Bathymetry of the Amundsen Sea Embayment sector of West Antarctica from Operation IceBridge gravity and other data. *Geophysical Research Letters*, *44*, 1360–1368. https://doi.org/10.1002/2016GL072071
Mills, M. M., Alderkamp, A.-C., Thurcózy, C.-E., van Dijken, G. L., Laan, P., de Baar, H., & Arrigo, K. R. (2012). Phytoplankton biomass and pigment responses to Fe amendments in the Pine Island and Amundsen polynyas. *Deep-Sea Research Part II*, *71-76*, 61–76.
Morales Maqueda, M. A., Willmott, A. J., & Biggs, N. R. T. (2004). Polynya dynamics: A review of observations and modeling. *Reviews of Geophysics*, *42*, RG1004. https://doi.org/10.1029/2002RG000116
Moreau, S., Lannuzel, D., Janssens, J., Arroyo, M. C., Corkill, M., Cougnon, E., et al. (2019). Sea ice meltwater and Circumpolar Deep Water drive contrasting productivity in three Antarctic polynyas. *Journal of Geophysical Research: Oceans*, *124*, 2943–2968. https://doi.org/10.1002/2019JC015071
Morel, F. M. M., Kustka, A. B., & Shaked, Y. (2008). The role of unchelated Fe in the iron nutrition of phytoplankton. *Limnology and Oceanography*, *53*, 400–404. https://doi.org/10.4319/lo.2008.53.1.0400
Nakayama, Y., Timmermann, R., Rodenhacke, C. B., Schröder, M., & Hellmer, H. H. (2014). Modeling the spreading of glacial meltwater from the Amundsen and Bellingshausen seas. *Geophysical Research Letters*, *41*, 7942–7949. https://doi.org/10.1002/2014GL061600
Naughten, K. A., Meissner, K. J., Galton-Fenzi, B. K., England, M. H., Timmermann, R., & Hellmer, H. H. (2018). Future projections of Antarctic ice shelf melting based on CMIP5 scenarios. *Journal of Climate*, *31*, 5243–5261. https://doi.org/10.1175/JCLI-D-17-0854.1
Nicholls, K. W., Østerhus, S., Makinson, K., Gammerlsrød, T., & Fahrback, E. (2009). Ice-ocean processes over the continental shelf of the southern Weddell Sea, Antarctica: A review. *Reviews of Geophysics*, *47*, RG3003. https://doi.org/10.1029/2007RG000250
Nicholls, K. W., Padman, L., Schröder, M., Woodgate, R. A., Jenkins, A., & Østerhus, S. (2003). Water mass modification over the continental shelf north of Ronne ice shelf, Antarctica. *Journal of Geophysical Research*, *108*(C8), 3260. https://doi.org/10.1029/2002JC001713
Niiler, P. P., & Kraus, E. B. (1977). One-dimensional models of the upper ocean. In E. B. Krauss (Ed.), *Modeling and prediction of the upper layers of the ocean*, (pp. 143–172). New York: Pergamon.
Nøst, O. A. (2004). Measurements of ice thickness and seabed topography under the Fimbul ice shelf, Dronning Maud Land, Antarctica. *Journal of Geophysical Research*, *109*, C10010. https://doi.org/10.1029/2004JC002277
Özturk, M., Bizsel, N., & Steinnes, E. (2003). Iron speciation in eutrophic and oligotrophic Mediterranean coastal waters; impact of phytoplankton and protozoan blooms on iron distribution. *Marine Chemistry*, *81*, 19–36. https://doi.org/10.1016/s0304-4203(02)00137-8
Paolo, F. S., Fricker, H. A., & Padman, L. (2015). Volume loss from Antarctic ice shelves is accelerating. *Science*, *348*(6232), 327–331. https://doi.org/10.1126/science.aaa0940
Person, R., Aumont, O., Madec, G., Vancoppenolle, M., Bopp, L., & Merino, N. (2019). Sensitivity of ocean biogeochemistry to the iron supply from the Antarctic ice sheet explored with a biogeochemical model. *Biogeosciences*, *16*, 3583–3603. https://doi.org/10.5194/bg-16-3583-2019
Piñones, A., Hofmann, E. E., Costa, D. P., Goetz, K., Burns, J. M., Roquet, F., et al. (2019). Hydrographic variability along the inner and mid-shelf region of the western Ross Sea obtained using instrumented seals. *Progress in Oceanography*, in press. https://doi.org/10.1016/j.pocean.2019.01.003
Potter, J. R., & Paren, J. G. (1985). Interaction between ice shelf and ocean in George VI Sound, Antarctica. In S. S. Jacobs (Ed.), *Oceanology of the Antarctic continental shelf*, *AGU Antarctic Research Series*, (Vol. 43, pp. 35–58). Washington, DC: American Geophysical Union.
Raiswell, R., Benning, L. G., Tranter, M., & Tulaczyk, S. (2008). Bioavailable iron in the Southern Ocean: The significance of the iceberg conveyor belt. *Geochem. T.*, *9*, 7. https://doi.org/10.1186/1467-4866-9-7
Randall-Goodwin, E., Meredith, M. P., Jenkins, A., Yager, P. L., Sherrell, R. M., Abrahamsen, E. P., et al. (2015). Freshwater distributions and water mass structure in the Amundsen Sea Polynya region, Antarctica. *Elementa: Science of the Anthropocene*, *3*, 65. https://doi.org/10.12952/journal.elementa.000065
Rignot, E., Jacobs, S., Mouginot, J., & Scheuchl, B. (2013). Ice shelf melting around Antarctica. *Science*, *341*(6143), 266–270. https://doi.org/10.1126/science.1235798
Rignot, E., and S.S. Jacobs, 2008: Ice-shelf melting around Antarctica. American Goephysical union, Fall Meeting, Abstract C41D-02.
Rignot, E. J. (1998). Fast recession of a West Antarctic glacier. *Science*, *281*(5376), 549–551. https://doi.org/10.1126/science.281.5376.549
Rossow, W.B., A.W. Walker, D.E. Beuschel, and M.D. Roiter, 1996: International Satellite Cloud Climatology Project (ISCCP) documentation of new cloud datasets. WMO/TD-no. 737, World Meteorological Organization, 115 pp.
Rubin, M., Berman-Frank, I., & Shaked, Y. (2011). Dust- and mineral-iron utilization by the marine dinitrogen-fixer *Trichodesmium*. *Nature Geoscience*, *4*, 529. https://doi.org/10.1038/ngeo1181
Schaffer, J., Timmermann, R., Arndt, J. E., Kristensen, S. S., Mayer, C., Morlighem, M., & Steinhage, D. (2016). A global, high-resolution data set of ice sheet topography, cavity geometry, and ocean bathymetry. *Earth System Science Data*, *8*, 543–557. https://doi.org/10.5194/essd-8-543-2016
Schmidtko, S., Heywood, K. J., Thompson, A. F., & Aoki, S. (2014). Multidecadal warming of Antarctic waters. *Science*, *346*, 1227–1231. https://doi.org/10.1126/science.1256117
Schroth, A. W., Crusius, J., Sholkovitz, E. R., & Bostick, B. C. (2009). Iron solubility driven by speciation in dust sources to the ocean. *Nature Geoscience*, *2*, 337–340. https://doi.org/10.1038/ngeo501
Sedwick, P. N., Bowie, A. R., & Trull, T. W. (2008). Dissolved iron in the Australian sector of the Southern Ocean (CLIVAR SR3 section): Meridional and seasonal trends. *Deep-Sea Research Part I*, *55*, 911–925. https://doi.org/10.1016/j.dsr.2008.03.011

Sedwick, P. N., Marsay, C. M., Sohst, B. M., Aguilar-Islas, A. M., Lohan, M. C., Long, M. C., et al. (2011). Early season depletion of dissolved iron in the Ross Sea polynya: Implications for iron dynamics on the Antarctic continental shelf. *Journal of Geophysical Research*, *116*, C12019. https://doi.org/10.1029/2010JC006553

Shchepetkin, A. F., & McWilliams, J. C. (2009). Correction and commentary for "ocean forecasting in terrain-following coordinate: Formulation and skill assessment of the regional ocean modeling system" by Haidvogel et al., 3595-3634. *Journal of Computational Physics*, *228*, 8985–9000. https://doi.org/10.1016/j.jcp.2009.09.002

Sherrell, R. M., Annett, A. L., Fitzsimmons, J. N., Roccanova, V. J., & Meredith, M. P. (2018). A "shallow bathtub ring" of local sedimentary iron input maintains the Palmer Deep biological hotspot on the West Antarctic Peninsula shelf. *Philosophical Transactions of the Royal Society A*, *376*. https://doi.org/10.1098/rsta.2017.0171

Sherrell, R. M., Lagerstrm, M. E., Forsch, K. O., Stammerjohn, S. E., & Yager, P. L. (2015). Dynamics of dissolved iron and other bioactive trace metals (Mn, Ni, Cu, Zn) in the Amundsen Sea Polynya, Antarctica. *Elementa: Science of the Anthropocene*, *3*, 71. https://doi.org/10.12952/journal.elementa.000071

Smetacek, V., & Nichol, S. (2005). Polar ocean ecosystems in a changing world. *Nature*, *437*(7057), 362–368. https://doi.org/10.1038/nature04161

Smethie, W. M., & Jacobs, S. S. (2005). Circulation and melting under the Ross ice shelf: Estimates from evolving CFC, salinity and temperature fields in the Ross Sea. *Deep Sea Research, Part I*, *52*, 959–978.

Smith, W. O., & Gordon, L. I. (1997). Hyperproductivity of the Ross Sea (Antarctica) polynya during austral spring. *Geophysical Research Letters*, *24*, 233–236.

Spolaor, A., Vallelonga, P., Cozzi, G., Gabrieli, J., Varin, C., Kehrwald, N., et al. (2013). Iron speciation in aerosol dust influences iron bioavailability over glacial-interglacial timescales. *Geophysical Research Letters*, *40*, 1618–1623. https://doi.org/10.1002/grl.50296

Steele, M., Mellor, G. L., & McPhee, M. G. (1989). Role of the molecular sublayer in the melting or freezing of sea ice. *Journal of Physical Oceanography*, *55*, 139–147.

Stern, A. A., Dinniman, M. S., Zagorodnov, V., Tyler, S. W., & Holland, D. M. (2013). Intrusion of warm surface water beneath the McMurdo ice shelf, Antarctica. *Journal of Geophysical Research: Oceans*, *118*, 7036–7048. https://doi.org/10.1002/2013JC008842

Stirling, I. (1997). The importance of polynyas, ice edges, and leads to marine mammals and birds. *Journal of Marine Systems*, *10*, 9–21.

St-Laurent, P., Yager, P. L., Sherrell, R. M., Oliver, H., Dinniman, M. S., & Stammerjohn, S. E. (2019). Modeling the seasonal cycle of iron and carbon fluxes in the Amundsen Sea polynya, Antartica. *Journal of Geophysical Research: Oceans*, *124*, 1544–1565. https://doi.org/10.1029/2018JC014773

St-Laurent, P., Yager, P. L., Sherrell, R. M., Stammerjohn, S. E., & Dinniman, M. S. (2017). Pathways and supply of dissolved iron in the Amundsen Sea (Antarctica). *Journal of Geophysical Research*, *122*, 7135–7162. https://doi.org/10.1002/2017JC013162

Tagliabue, A. (2014). More to hydrothermal iron input than meets the eye. *Proceedings of the National Academy of Sciences*, *111*, 16641–16642. https://doi.org/10.1073/pnas.1419829111

Tagliabue, A., Aumont, O., DeAth, R., Dunne, J. P., Dutkiewicz, S., Galbraith, E., et al. (2016). How well do global ocean biogeochemistry models simulate dissolved iron distributions? *Global Biogeochemical Cycles*, *30*, 149–174. https://doi.org/10.1002/2015GB005289

Tagliabue, A., Bopp, L., Dutay, J. C., Bowie, A. R., Chever, F., Jean-Baptiste, P., et al. (2010). Hydrothermal contribution to the oceanic dissolved iron inventory. *Nature Geoscience*, *3*, 252–256. https://doi.org/10.1038/ngeo818

Tagliabue, A., & Resing, J. (2016). Impact of hydrothermalism on the ocean iron cycle. *Philosophical Transactions of the Royal Society A*, *374*(20), 150–291. https://doi.org/10.1098/rsta.2015.0291

Timmermann, R., & Hellmer, H. H. (2013). Southern Ocean warming and increased ice shelf basal melting in the 21st and 22nd centuries based on coupled ice-ocean finite-element modeling. *Ocean Dynamics*, *63*, 1011. https://doi.org/10.1007/s10236-013-0642-0

van der Merwe, P., Wuttig, K., Holmes, T., Trull, T. W., Chase, Z., Townsend, A. T., et al. (2019). High lability Fe particles sourced from glacial EROSION can meet previously unaccounted biological demand: Heard Island, Southern Ocean. *Frontiers in Marine Science*, *6*, 332. https://doi.org/10.3389/fmars.2019.00332

von der Heyden, B. P., Roychoudhury, A. N., Mtshali, T. N., Tyliszczak, T., & Myneni, S. C. B. (2012). Chemically and geographically distinct solid-phase iron pools in the Southern Ocean. *Science*, *338*(6111), 1199–1201. https://doi.org/10.1126/science.1227504

Wagener, T., Guieu, C., Losno, R., Bonnet, S., & Mahowald, N. (2008). Revisiting atmospheric dust export to the Southern Hemisphere ocean: Biogeochemical implications. *Global Biogeochemical Cycles*, *22*, GB2006. https://doi.org/10.1029/2007GB002984

Wen, J., Wang, Y., Wang, W., Jezek, K. C., Liu, H., & Allison, I. (2010). Basal melting and freezing under the Amery ice shelf, East Antarctica. *Journal of Glaciology*, *56*, 81–90. https://doi.org/10.3189/002214310791190820

Yager, P. L., Sherrell, R. M., Stammerjohn, S. E., Ducklow, H. W., Schofield, O. M. E., Ingall, E. D., et al. (2016). A carbon budget for the Amundsen Sea polynya, Antarctica: Estimating net community production and export in a highly productive polar ecosystem. *Elementa: Science of the Anthropocene*, *4*, 140. https://doi.org/10.12952/journal.elementa.000140

Yu, J., Liu, H., Jezek, K. C., Warner, R. C., & Wen, J. (2010). Analysis of velocity field, mass balance, and basal melt of the Lambert glacier–Amery ice shelf system by incorporating Radarsat SAR interferometry and ICESat laser altimetry measurements. *Journal of Geophysical Research*, *115*, B11102. https://doi.org/10.1029/2010JB007456

Zhu, Z., Xu, K., Fu, F., Spackeen, J. L., Bronk, D. A., & Hutchins, D. A. (2016). A comparative study of iron and temperature effects on diatoms and *Phaeocystis Antarctica* from the Ross Sea, Antarctica. *Marine Ecology Progress Series*, *550*, 39–51. https://doi.org/10.3354/meps11732